Article

Cell

Anti-CRISPR-Associated Proteins Are Crucial Repressors of Anti-CRISPR Transcription

Graphical Abstract

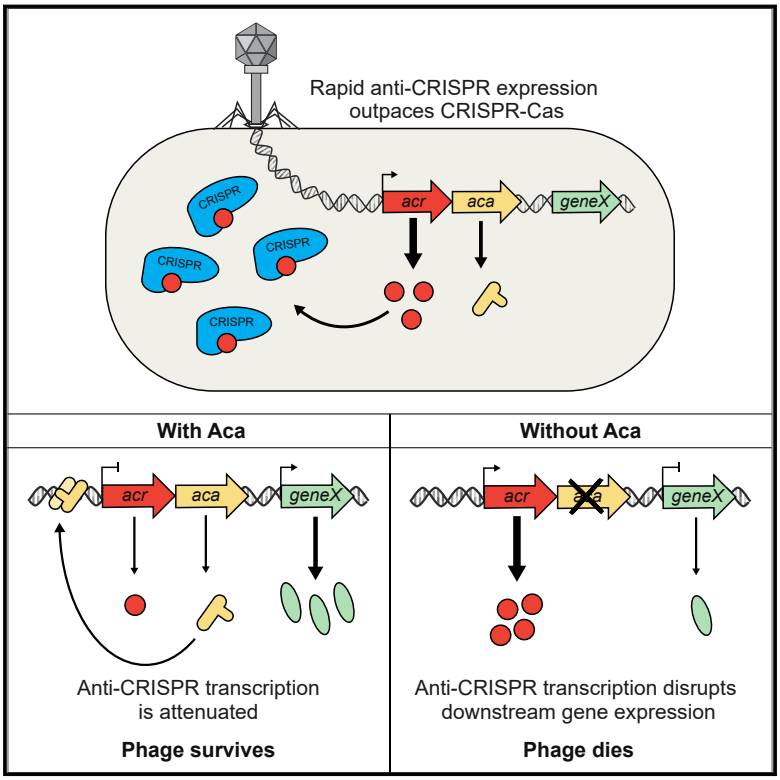

Highlights

- Anti-CRISPR genes are transcribed to high levels quickly after phage infection
- Aca proteins are ubiquitous DNA-binding proteins encoded in anti-CRISPR operons
- Aca proteins repress anti-CRISPR transcription
- Aca function obviates deleterious effects of high anti-CRISPR transcription

Authors

Sabrina Y. Stanley, Adair L. Borges, Kuei-Ho Chen, Danielle L. Swaney, Nevan J. Krogan, Joseph Bondy-Denomy, Alan R. Davidson

Correspondence

alan.davidson@utoronto.ca

In Brief

Anti-CRISPR-associated (Aca) proteins function as repressors of anti-CRISPR transcription.

Stanley et al., 2019, Cell *178*, 1–13
September 5, 2019
https://doi.org/10.1016/j.cell.2019.07.046

CellPress

Please cite this article in press as: Stanley et al., Anti-CRISPR-Associated Proteins Are Crucial Repressors of Anti-CRISPR Transcription, Cell (2019), https://doi.org/10.1016/j.cell.2019.07.046

Article

Cell

Anti-CRISPR-Associated Proteins Are Crucial Repressors of Anti-CRISPR Transcription

Sabrina Y. Stanley,[1] Adair L. Borges,[2] Kuei-Ho Chen,[3] Danielle L. Swaney,[3,4,5] Nevan J. Krogan,[3,4,5] Joseph Bondy-Denomy,[2,4] and Alan R. Davidson[1,6,7,*]

[1]Department of Molecular Genetics, University of Toronto, Toronto, ON M5S 1A8, Canada
[2]Department of Microbiology and Immunology, University of California, San Francisco, San Francisco, CA 94143, USA
[3]The J. David Gladstone Institutes, San Francisco, CA 94158 USA
[4]Quantitative Biosciences Institute, University of California, San Francisco, San Francisco, CA 94143, USA
[5]Department of Cellular and Molecular Pharmacology, University of California, San Francisco, San Francisco, CA 94143, USA
[6]Department of Biochemistry, University of Toronto, Toronto, ON M5S 1A8, Canada
[7]Lead Contact
*Correspondence: alan.davidson@utoronto.ca
https://doi.org/10.1016/j.cell.2019.07.046

SUMMARY

Phages express anti-CRISPR (Acr) proteins to inhibit CRISPR-Cas systems that would otherwise destroy their genomes. Most *acr* genes are located adjacent to anti-CRISPR-associated (*aca*) genes, which encode proteins with a helix-turn-helix DNA-binding motif. The conservation of *aca* genes has served as a signpost for the identification of *acr* genes, but the function of the proteins encoded by these genes has not been investigated. Here we reveal that an *acr*-associated promoter drives high levels of *acr* transcription immediately after phage DNA injection and that Aca proteins subsequently repress this transcription. Without Aca activity, this strong transcription is lethal to a phage. Our results demonstrate how sufficient levels of Acr proteins accumulate early in the infection process to inhibit existing CRISPR-Cas complexes in the host cell. They also imply that the conserved role of Aca proteins is to mitigate the deleterious effects of strong constitutive transcription from *acr* promoters.

INTRODUCTION

CRISPR-Cas systems immunize bacteria and archaea against invading genetic elements like phages by incorporating short sequences of DNA from these invaders into their chromosome (Datsenko et al., 2012; Levy et al., 2015; Yosef et al., 2012). These sequences are transcribed and processed into small RNAs known as CRISPR RNAs (crRNAs) that bind to CRISPR-associated (Cas) proteins to form ribonucleoprotein interference complexes. These complexes survey the cell, recognize foreign nucleic acids through complementarity with their crRNAs, and ultimately destroy them through the intrinsic nuclease activity of the Cas proteins (Barrangou et al., 2007; Brouns et al., 2008; Garneau et al., 2010; Marraffini and Sontheimer, 2008). CRISPR-Cas systems are diverse, comprising six distinct types, each with multiple subtypes (Makarova et al., 2015). In many bacteria, CRISPR-Cas systems are expressed in the absence of phage infection (Agari et al., 2010; Cady et al., 2011; Deltcheva et al., 2011; Juranek et al., 2012; Young et al., 2012), ensuring that they are always primed to defend against a previously encountered phage.

In response to CRISPR-Cas, phages and other mobile genetic elements endure by encoding protein inhibitors of CRISPR-Cas systems, known as anti-CRISPRs (Bondy-Denomy et al., 2013; Pawluk et al., 2016b). Anti-CRISPRs are encoded in diverse viruses and mobile elements found in the Firmicutes, Proteobacteria, and Crenarchaeota phyla. They show a tremendous amount of sequence diversity, with over 40 entirely distinct anti-CRISPR protein families now identified. Among these families are inhibitors of type I-C, I-D, I-E, I-F, II-A, II-C, and V-A systems. These anti-CRISPR proteins function by preventing CRISPR-Cas systems from recognizing foreign nucleic acids or by inhibiting their nuclease activity (Bondy-Denomy et al., 2015; Chowdhury et al., 2017; Dong et al., 2017, 2019; Guo et al., 2017; Harrington et al., 2017; Knott et al., 2019; Pawluk et al., 2017; Wang et al., 2016).

Anti-CRISPR proteins display no common features with respect to the sequence, predicted structure, or genomic location of the genes encoding them. However, anti-CRISPR genes are almost invariably found upstream of a gene encoding a protein containing a helix-turn-helix (HTH) DNA-binding domain (Figure 1). Seven different families of genes encoding these HTH-containing proteins have been designated anti-CRISPR-associated (*aca*). Members of the *aca* gene families have been identified in phages, prophages, plasmids, and conjugative elements in diverse bacterial species (Bondy-Denomy et al., 2013; Marino et al., 2018; Pawluk et al., 2016a, 2016b). The ubiquity of *aca* genes adjacent to anti-CRISPR genes has provided a key bioinformatic tool for the identification of diverse anti-CRISPR families (Marino et al., 2018; Pawluk et al., 2016a, 2016b) and implies that they play an important role in anti-CRISPR systems. Nevertheless, their function remains unknown.

The goal of this work was to define the role of *aca* genes in anti-CRISPR biology. We investigated *aca* gene function using *Pseudomonas aeruginosa* phage JBD30 as our primary model system (Figure 1). This phage was among the first set of phages shown to use an anti-CRISPR gene for survival in the presence of

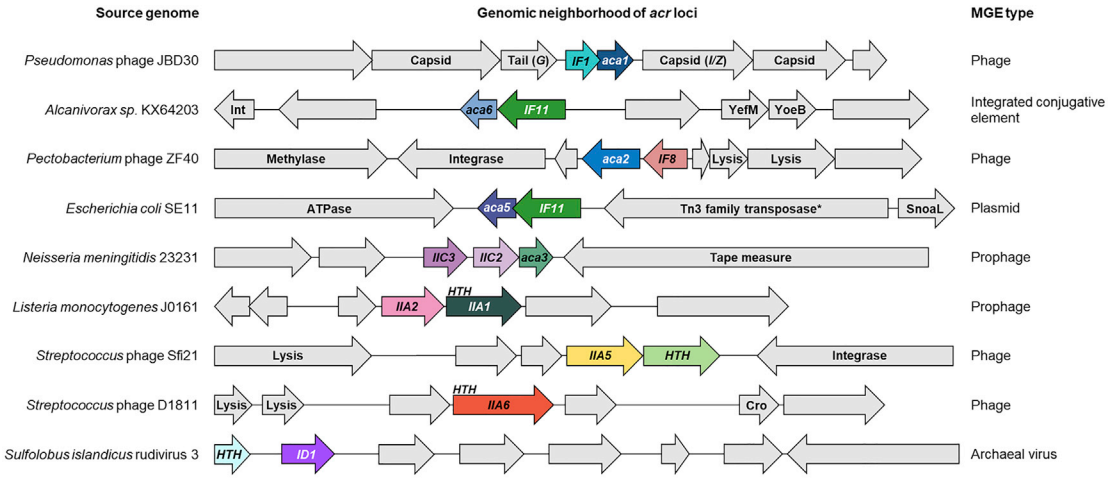

Figure 1. Anti-CRISPRs Are Found in Diverse Genomic Contexts

Shown is a schematic representation of the genomic context of diverse anti-CRISPR genes. Colored arrows represent anti-CRISPR and anti-CRISPR-associated (*aca*) genes as well as nearby genes encoding helix-turn-helix (HTH) motif proteins. Genes shown in the same color represent the same family. Other genes are shown in gray, and predicted functions are indicated when known. Arrows representing genes are not shown to scale. *G* encodes a phage tail protein, and *I/Z* encodes the protease/scaffold. Int, integrase. *, frameshifted/incomplete. Anti-CRISPR genes are denoted as *IX#*, where I represents the type of system targeted, X represents the subtype of system targeted, and # represents the protein family. See also Figure S7 and Table S2.

CRISPR-Cas (Bondy-Denomy et al., 2013). The anti-CRISPR operon of JBD30 and other closely related phages is located between operons encoding phage structural proteins. In JBD30, a single anti-CRISPR (*acr*) gene, *acrIF1*, is followed directly by an *aca* gene known as *aca1*. Aca1 is conserved (>50% identity) among diverse anti-CRISPR-encoding phages and prophages in *Pseudomonas* species (Pawluk et al., 2016b). Because Aca1 possesses a HTH DNA-binding motif, we reasoned that it might be involved in regulating anti-CRISPR gene transcription. To address this, we investigated the transcript levels of the *acrIF1* gene of JBD30 throughout its infection cycle. We found that anti-CRISPR transcription occurs at a high level early in the phage infection process and that Aca1 represses this transcription. Remarkably, we found that the repressor activity of Aca1 is essential for phage survival irrespective of CRISPR-Cas. We also showed that other Aca protein families act as repressors of anti-CRISPR transcription. This crucial function of Aca likely explains its ubiquity in anti-CRISPR operons.

RESULTS

The *acrIF1* Gene Is Robustly Transcribed from Its Own Promoter at the Onset of Phage Infection

To investigate the potential role of Aca1 in regulating *acr* transcription, we first evaluated the dynamics of anti-CRISPR gene expression over the course of phage infection in *P. aeruginosa* strain PA14, which encodes a type I-F CRISPR-Cas system. A lysate of phage JBD30 was mixed with PA14, and samples were removed at successive time points after phage addition. By extracting RNA from these samples, which span the lytic cycle of JBD30 (~70 min; Figure S1) and quantifying the level of anti-CRISPR *acrIF1* transcripts using qRT-PCR, we found that *acrIF1* transcription was easily detectable within 6 min after infection (Figure 2A). There was a more than 100-fold increase in the level of anti-CRISPR transcripts within the first 20 min of infection. Remarkably, *acrIF1* transcription initiated earlier and at a considerably higher level than that of the transposase gene (*A*), which is expected to be one of the first genes transcribed in JBD30. JBD30 is very similar to the well-characterized *E. coli* phage Mu in its genome organization and composition, placing it in the Mu-like phage family. The transposase is expressed early in infection because it is required for the first step in the life cycle of Mu-like phages, which involves transposition of the phage genome into that of the host (Marrs and Howe, 1990). Also, by comparison with phage Mu, we expected transcription of gene *G*, a gene required for phage morphogenesis located directly upstream of the *acrIF1* gene, to increase late in the infection process. In accord with this expectation, the *G* transcript did not accumulate to appreciable levels until 50 min after phage addition. Overall, these data show that *acrIF1* transcription is very high early in the infection process, presumably allowing the anti-CRISPR protein to accumulate sufficiently to inhibit the pre-formed CRISPR-Cas complexes present in the cell.

The distinct transcription profile of the *acrIF1* gene implied that it possessed its own promoter. A DNA sequence alignment of the region upstream of diverse *acr* genes from phages related to JBD30 revealed a conserved predicted promoter (Figure 2B). This region from phage JBD30 was cloned upstream of a promoterless *lacZ* reporter gene carried on a plasmid. The presence of the putative *acrIF1* promoter increased β-galactosidase activity by approximately 15-fold compared with the control lacking a promoter, demonstrating that this DNA sequence can direct robust transcription in *P. aeruginosa* (Figure 2C). To confirm that this promoter was responsible for anti-CRISPR gene expression during phage infection, we created a JBD30 mutant phage (JBD30ΔP*acr*) lacking this region. In a plaquing assay, the JBD30ΔP*acr* mutant phage replicated robustly on PA14

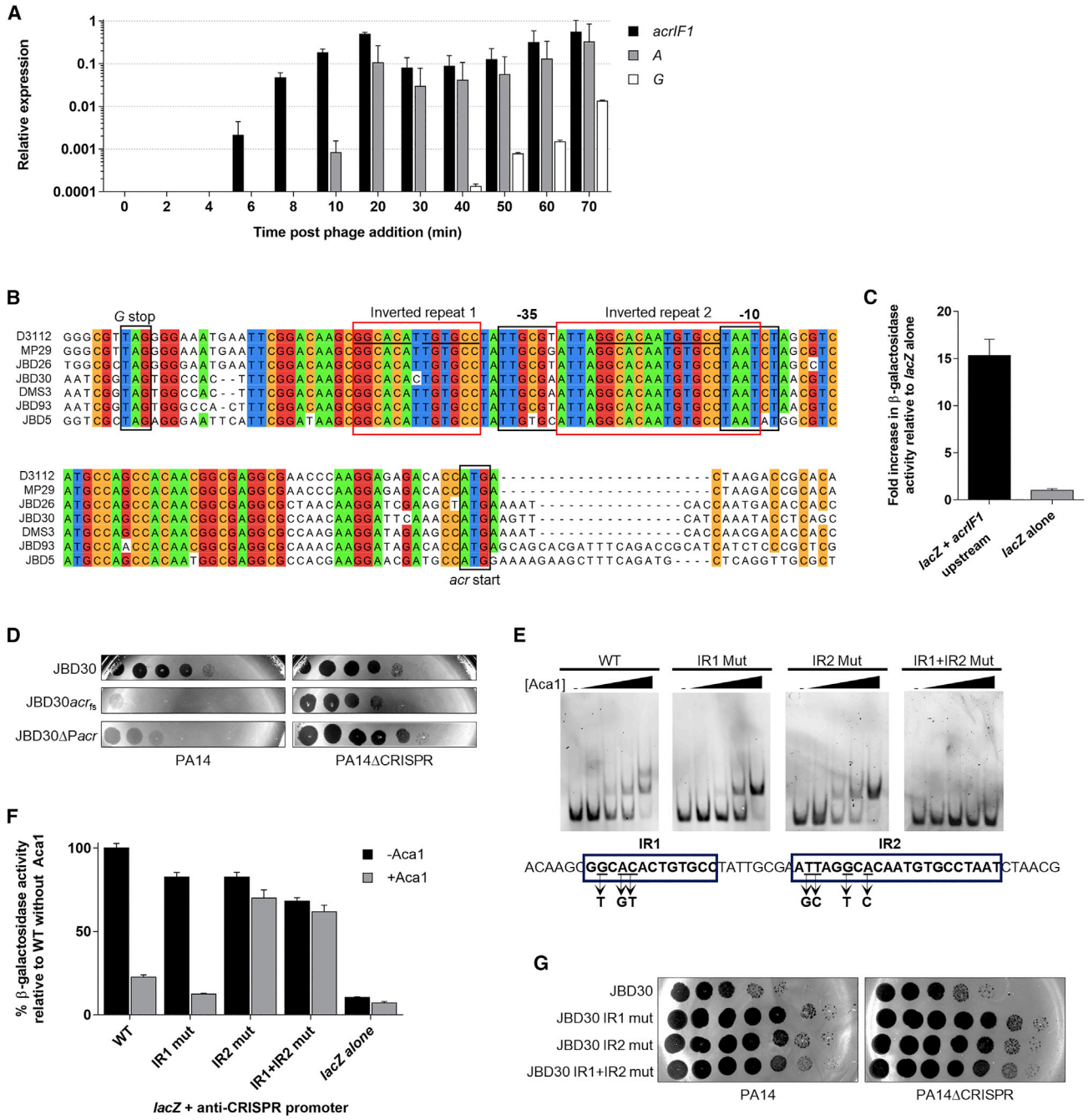

Figure 2. *acrIF1* Expression Is Driven by a Promoter Region that Includes Binding Sites for Aca1

(A) Relative transcription levels of phage genes were measured by qRT-PCR at the indicated times after infection of PA14 by phage JBD30. Transcriptional levels are shown of the anti-CRISPR gene (*acrIF1*), an early-expressed gene (*A*, transposase), and a late-expressed gene (*G*, a tail component) during one round of phage infection at an MOI of 5. Levels were normalized to the geometric mean of the transcript levels of the housekeeping genes *clpX* and *rpoD*. Data are represented as mean ± SEM from three independent experiments.

(B) Multiple nucleotide sequence alignment of anti-CRISPR phages from the stop codon of the Mu *G* homolog (*G* stop) to the start codon of the anti-CRISPR genes (*acr* start). Bioinformatically predicted promoter elements (BPROM; Solovyev and Salamov, 2011) −10 and −35 are shown. Inverted repeats are indicated by red boxes. A common sequence in both repeats is underlined. Positions sharing more than 85% identity are colored according to nucleotide.

(C) The putative *acr* promoter region from phage JBD30 was cloned upstream of a promoterless *lacZ* expression vector (*lacZ+acrIF1* upstream), and β-galactosidase activity was measured in *P. aeruginosa* strain PA14. The mean ± SEM of three independent assays is shown.

(D) 10-fold dilutions of wild-type (JBD30), anti-CRISPR gene frameshift mutant (JBD30*acr*$_{fs}$), and *acr* promoter mutant (JBD30ΔP*acr*) phage lysates were applied to lawns of PA14 and PA14ΔCRISPR.

(legend continued on next page)

lacking a functional CRISPR-Cas system (PA14ΔCRISPR), but in the presence of CRISPR-Cas, phage replication was equivalent to that of a JBD30 mutant bearing a frameshift mutation in *acrIF1* (acr_{fs}) (Figure 2D). These data imply that the identified promoter drives *acrIF1* transcription during infection.

Aca1 Acts on the *acr* Promoter

Aca1 proteins are bioinformatically predicted to contain a HTH DNA-binding motif (Figure S2A). HTH-containing proteins are generally dimeric and bind to inverted repeat sequences (Luscombe et al., 2000). We identified two such sites with very similar sequences, to which we refer as inverted repeat 1 (IR1) and inverted repeat 2 (IR2). IR1 lies upstream of the −35 region of the *acrIF1* promoter, and IR2 lies between the −35 and −10 regions (Figure 2B). To determine whether Aca1 could bind to the *acr* promoter region, purified Aca1 was mixed with a 110-bp dsDNA fragment containing the *acr* promoter, and an electrophoretic mobility shift assay (EMSA) was performed. Incubation of the promoter-containing fragment with Aca1 resulted in a concentration-dependent shift in the mobility of the fragment, which was not observed with a non-specific DNA sequence (Figure S2B). At higher Aca1 concentrations, a second shifted band was observed, consistent with the presence of two Aca1 binding sites within this fragment. The K_D of this interaction was approximately 50 nM (Figure S2C). This K_D value is 10- to 100-fold weaker than those of other well-known HTH-containing proteins (Gilbert and Müller-Hill, 1967; Kamionka et al., 2004; Liu and Matthews, 1993; Nelson and Sauer, 1985). A 53-bp fragment encompassing only IR1 and IR2 of the *acr* promoter was also bound by Aca1 and displayed two shifted bands by EMSA (Figure 2E). To determine whether the two shifted bands represented Aca1 binding at both IR1 and IR2 sites, point mutations were introduced into each inverted repeat to abolish their symmetry. Fragments bearing mutations in either IR1 or IR2 still bound to Aca1, but only a single shifted band was observed, whereas no shift was observed with a fragment bearing mutations in both sites. These results demonstrated that Aca1 binds the *acrIF1* promoter at both the IR1 and IR2 sites.

Given the binding of Aca1 to the *acrIF1* promoter and the position of IR1 relative to the core promoter elements, we speculated that Aca1 might contribute to the strong transcription of the anti-CRISPR gene early in infection. To determine whether Aca1 binding to the *acrIF1* promoter modulates its transcriptional activity, we measured the activity of this promoter in the presence of Aca1 using the *lacZ* reporter assay described above. Contrary to our expectation, the presence of Aca1 led to a 5-fold reduction in β-galactosidase reporter activity (Figure 2F). The repressive activity of Aca1 depended on the presence of an intact IR2 site, suggesting that this site is active *in vivo*. By contrast, the IR1 site was not required for repression despite being bound by Aca1 *in vitro*. The *in vivo* function of the Aca1 binding sites in the *acrIF1* promoter were assessed by crossing the inverted repeat mutations into phage JBD30 through *in vivo* recombination (Bondy-Denomy et al., 2013). Despite the marked effect of the IR1 and IR2 mutations on Aca1 DNA binding *in vitro*, introduction of these mutations into the phage genome caused no significant decrease in the viability of the mutant phages on either PA14 or PA14ΔCRISPR (Figure 2G).

Aca1 Repressor Activity Is Required for Phage Viability

To further investigate the role of Aca1 DNA-binding activity, we introduced amino acid substitutions within the putative HTH region of Aca1 that were expected to reduce DNA binding Figures S2A and S2D). Substitutions with Ala at Arg33 or Arg34 and an Arg33/Arg34 double mutant each partially reduced the DNA-binding activity of Aca1 *in vitro*, whereas substituting Arg44, which is predicted to be in the major groove recognition helix, completely abolished Aca1 DNA binding (Figure 3A). The DNA-binding activity of these mutants was also measured using the *lacZ* reporter assay. Consistent with the *in vitro* data, the R44A mutant displayed very little repressor activity on the *acrIF1* promoter (Figure 3B). The activity of the R33A/R34A double mutant was intermediate between the R44A mutant and the R33A and R34A single mutants, corroborating the *in vitro* changes in DNA-binding activity observed for these mutants.

The Aca1 DNA-binding mutants were subsequently crossed into phage JBD30. Unexpectedly, we were able to isolate phages carrying the mutations affecting Arg33 and Arg34 but not the mutation affecting Arg44. The R44A mutant phage could only be obtained by plating on cells expressing wild-type Aca1 from a plasmid, suggesting that the Aca1 DNA-binding activity is essential for phage viability. Using high-titer lysates of JBD30*aca1*^{R44A} produced in the presence of Aca1, we discovered that this phage was unable to replicate (titer reduced more than 10^6-fold) on PA14 or PA14ΔCRISPR (Figure 3C). By contrast, the mutant phages encoding Aca1 substitutions at the Arg33 or Arg34 positions formed plaques at levels approaching that of the wild-type phage (Figure S3A). These data demonstrate that intermediate reductions of Aca1 DNA-binding activity have little effect on phage viability but that complete loss of Aca1 DNA-binding activity is lethal.

Although the JBD30*aca1*^{R44A} phage replicated very poorly on the PA14ΔCRISPR strain, plating high concentrations of this phage did lead to the appearance of revertant plaques at a low frequency ($<1 \times 10^{-6}$). Sequencing the anti-CRISPR regions of several of these revertants revealed that they still carried the

(E) EMSAs were performed using a dsDNA fragment with the sequence shown, which encompasses the *acr* promoter region. The IR1 and IR2 mutants contained the triple and quadruple base substitutions indicated under the DNA sequence. Representative non-denaturing polyacrylamide gels stained with SYBR Gold are shown. Purified Aca1 was added to the DNA at concentrations of 10 nM, 50 nM, 100 nM, and 250 nM. The dash indicates no added protein.

(F) The *acr* promoter region from JBD30, either wild-type (WT) or bearing IR1 and/or IR2 mutations, was cloned upstream of a promoterless *lacZ* gene. β-Galactosidase activity was measured in PA14 (−Aca1) or in a JBD30 lysogen (+Aca1). The mean ± SEM β-galactosidase activity relative to the wild-type promoter is shown ($n \geq 3$).

(G) 10-fold dilutions of phage JBD30 lysates carrying the indicated inverted repeat mutations were applied to lawns of PA14 or PA14ΔCRISPR. Representative images of three replicates are shown.

See also Figures S1 and S2.

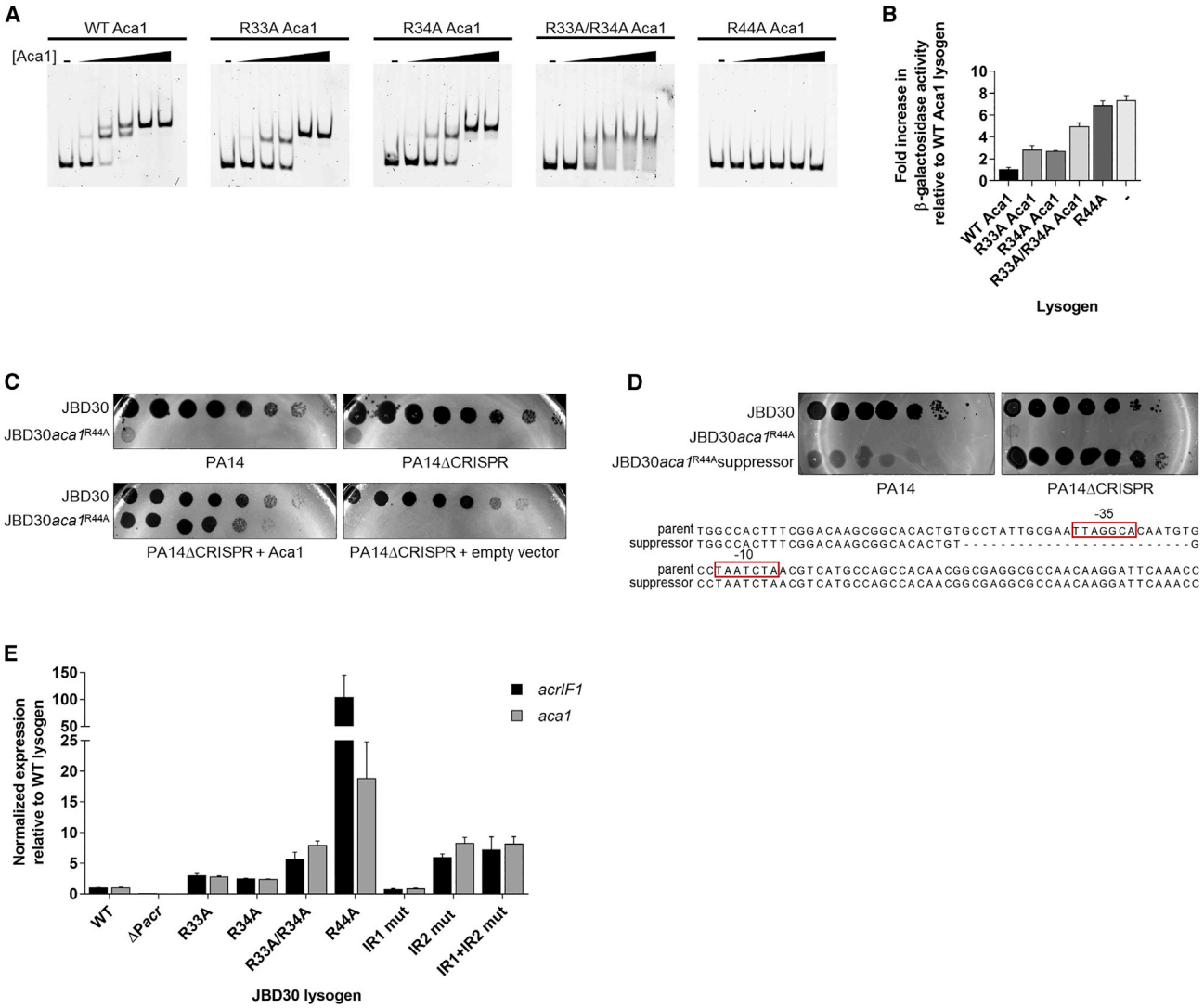

Figure 3. Uncontrolled Expression from the Anti-CRISPR Promoter Is Detrimental to Phage Viability

(A) Representative EMSA with the indicated Aca1 mutants using the 110-bp upstream region from phage JBD30 as a substrate. Purified protein was added at concentrations of 10 nM, 50 nM, 100 nM, 250 nM, and 500 nM. The dash indicates no added protein. Non-denaturing acrylamide gels stained with SYBR Gold are shown.

(B) The *acr* promoter region from phage JBD30 was cloned upstream of a promoterless *lacZ* gene. β-Galactosidase activity was measured in a wild-type JBD30 lysogen (WT Aca1), JBD30 Aca1 mutant lysogens as indicated, and wild-type PA14 with no prophage (−). The mean ± SEM from three independent experiments relative to the wild-type Aca1 JBD30 lysogen is shown.

(C) Lysates of phage JBD30 (WT or Aca1 R44A mutant) were spotted in 10-fold serial dilutions on lawns of PA14 or PA14ΔCRISPR or on PA14ΔCRISPR bearing a plasmid that expresses Aca1. These phages are targeted by the CRISPR-Cas system in the absence of anti-CRISPR activity. Representative images from three replicates are shown.

(D) Lysates of wild-type JBD30, JBD30*aca1*^{R44A} mutant phages, and suppressor JBD30*aca1*^{R44A} phages were spotted in 10-fold serial dilutions on bacterial lawns of PA14 or on PA14ΔCRISPR. The sequence of the suppressor phage demonstrating loss of the −35 element from the *acr* promoter compared with the sequence of the parent phage is shown below.

(E) The transcript levels of the *acrIF1* and *aca1* genes in phages bearing *acr* promoter operator mutants and *aca* mutants were determined by qRT-PCR. Expression levels were normalized to the geometric mean of the transcript levels of two bacterial housekeeping genes: *clpX* and *rpoD*. The mean ± SEM is shown (n = 3). Assays were performed in PA14ΔCRISPR lysogens of the indicated phages.

See also Figure S2 and S3.

aca1^{R44A} mutation. Most also displayed a 25-bp deletion encompassing the −35 region of the *acrIF1* promoter (Figure 3D). These suppressors were able to plate to the same level as wild-type JBD30 on the PA14ΔCRISPR strain but showed a marked reduction in titer on PA14. This is what we would expect to see if the *acr* promoter were impaired, as demonstrated in Figure 2D. This

result implies that the inviability of the *aca1*^{R44A} mutant phage likely arises from the high transcription level at the *acr* promoter. Hence, deletion of a critical portion of this promoter is able to restore viability.

To verify the transcriptional effects of mutations in the JBD30 *acr* promoter and *aca1* gene, we performed qRT-PCR on strains lysogenized with mutant phages (i.e., the phage genomes were integrated into the PA14ΔCRISPR genome to form a prophage). In the lysogenic state, *acr* expression must persist to prevent the host CRISPR-Cas system from targeting the prophage, which would be lethal. Performing assays in the lysogenic state also allowed us to assess transcription levels at a steady state as opposed to the dynamic situation existing during phage infection. Both the *acrIF1* and *aca1* genes were transcribed from the JBD30 prophage (Figure 3E). The transcription of both genes was more than 20-fold lower in the phage mutant lacking the *acr* promoter, confirming the key role of this promoter in expression of both of these genes. By contrast, the JBD30*aca1*^{R44A} mutant displayed vastly increased levels of *acrIF1* and *aca1* transcription (100-fold and 20-fold increases, respectively). Prophages expressing Aca1 mutants that bound DNA at somewhat reduced levels *in vitro* (i.e., substitutions at Arg33 and Arg34; Figure 3A) also displayed increased transcription of the *acrIF1* and *aca1* genes but not nearly to the same degree as the JBD30*aca1*^{R44A} mutant. Mutations in IR2 that that caused loss of repression in the *lacZ* reporter assay (Figure 2F) also resulted in increased *acrIF1* and *aca* transcription. However, this increase was similar to that of the JBD30*aca1*$^{R33A/R34A}$ mutant, which was 15-fold lower than that of the JBD30*aca1*^{R44A} mutant. The reduced transcription level of the IR2 and IR1+IR2 operator mutants compared with the transcription level of the *aca1*^{R44A} mutant may be due to the base substitutions in the operators causing a reduction in promoter strength. We investigated this issue by combining the IR1+IR2 operator mutant with *aca1*^{R44A} within the phage. This mutant phage was fully viable on the PA14Δ CRISPR strain (Figure S3B), consistent with the mutations in the Aca1 operator sites also reducing promoter strength. This result also explains why the IR1+IR2 operator mutant phage is viable even though Aca1 cannot repress this promoter.

Taken together, our data imply that the uniquely high transcription level from the *acr* promoter resulting from the *aca1*^{R44A} mutant causes the inviability of the JBD30*aca1*^{R44A} phage, whereas phages bearing other *aca1* or *acr* promoter mutations retained their replicative ability. It is notable that examination of plaque sizes resulting from infection by wild-type and JBD30 phages bearing other *aca1* mutations showed that the Arg33 and Arg34 substitutions measurably decreased phage replication (Figure S3C). Thus, the more modest increases in *acr* promoter activity seen for these mutants still influenced phage viability.

Although our results using the *aca1*^{R44A} mutant suggest that the key role of Aca1 is to repress *acr* transcription, it is possible that the lethal effect of this mutant could have been the result of a toxic gain of function. To rule out this scenario, we plated phages on cells expressing the Aca1 R44A mutant from the *acrIF1* promoter on a high-copy-number plasmid. This high expression of the Aca1 R44A mutant prior to phage infection had no effect on phage viability (Figure S3D). Plasmid-based overexpression of AcrIF1 in the same manner also had no effect on phage viability, implying that the non-viability of JBD30*aca1*^{R44A} is not due to lethal overaccumulation of Aca1 R44A or AcrIF1.

acr Promoter Activity Is Strong during Early Infection, Independent of Aca1

To directly address the role of Aca1 early in the phage infection process, we infected cells with wild-type JBD30 or the JBD30*aca1*^{R44A} mutant and measured transcript accumulation using qRT-PCR. Very early in infection, *acrIF1* transcripts accumulated to high levels in both wild-type and mutant phages (Figure 4A). At the 30- and 40-min time points, *acrIF1* transcripts accumulated to levels 85- to 140-fold higher, respectively, in the JBD30*aca1*^{R44A} mutant compared with the wild-type, highlighting the repressor activity of Aca1. The transcription of the transposase gene varied relatively little between the wild-type and mutant phages (Figure 4B). It should be noted that transcription of both the *acrIF1* and transposase genes was observed earlier in these experiments than in those shown in Figure 2A because of the use of a higher multiplicity of infection (MOI) to improve the limit of detection in this assay. These results clearly demonstrate that Aca1 is not required for early activation of *acr* transcription. Consequently, the importance of Aca1 must be derived from its ability to repress the *acr* promoter.

Loss of Aca1 Repressor Activity Alters the Transcription of Downstream Genes

In light of the results above, we postulated that the loss of viability observed for the JBD30*aca1*^{R44A} mutant was brought about by uncontrolled transcription from the strong *acr* promoter. With the expectation that this inappropriate *acr* transcription might perturb the transcription of downstream genes, we measured the transcript levels of the phage protease/scaffold (*I/Z*) gene, which lies immediately downstream of the anti-CRISPR locus. Surprisingly, *I/Z* gene transcript levels in the JBD30*aca1*^{R44A} mutant phages were dramatically decreased relative to wild-type phages, reaching a nearly 100-fold difference at the later time points (Figure 4C). By contrast, the *G* gene, which lies immediately upstream of the anti-CRISPR locus, displayed less than 10-fold differences in transcript levels between the wild-type and mutant phages (Figure 4D).

Based on genomic comparison with phage Mu, the *I/Z* gene is situated at the beginning of an operon that contains genes required for capsid morphogenesis (Hertveldt and Lavigne, 2008). The observed decrease in *I/Z* transcript level likely extends to other essential genes within this operon. Thus, the JBD30*aca1*^{R44A} mutant phage would lack sufficient levels of these morphogenetic proteins required for particle formation. This explains the observed loss of phage viability regardless of the CRISPR-Cas status of the host. Defects in virion morphogenesis could also lead to the small plaque phenotype observed in the partially incapacitated Aca1 mutants (Figure S3C). In further experiments, we determined that the JBD30*aca1*^{R44A} phage forms lysogens with the same frequency as the wild-type phage (Figure S4). Because lysogen formation does not require particle formation, this finding is consistent with the hypothesis that Aca1 debilitation causes a defect in phage morphogenesis in the case of JBD30.

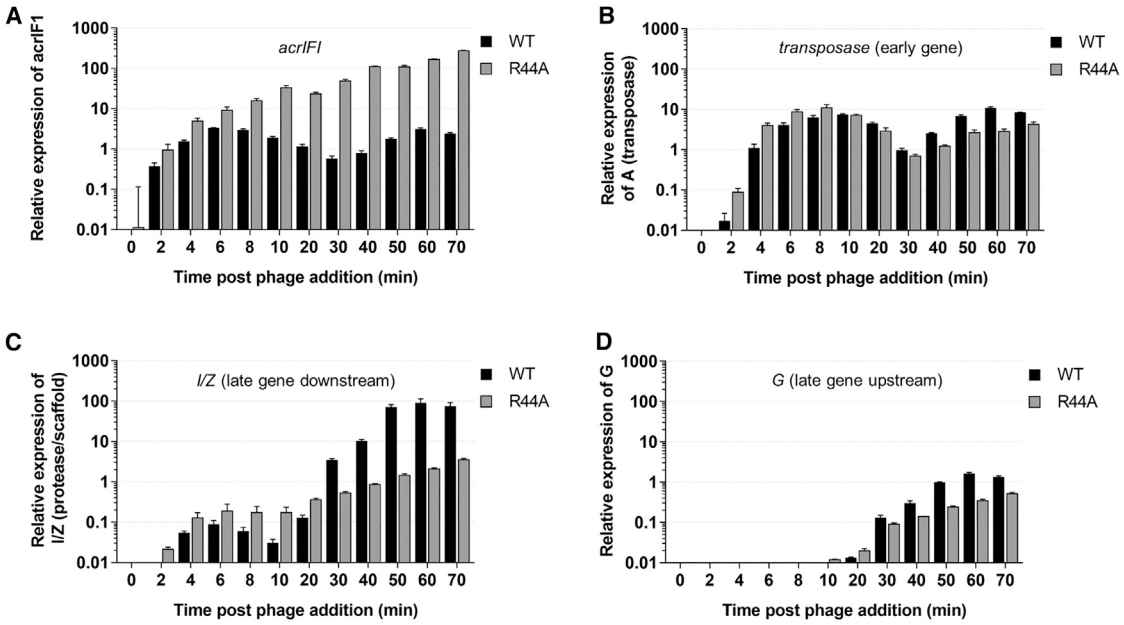

Figure 4. Loss of Aca1 Repressor Activity Affects the Transcription of the Gene Immediately Downstream of the Anti-CRISPR Locus

(A–D) The transcription of the indicated phage genes from wild-type JBD30 and JBD30*aca1*^{R44A} during one round of infection was determined by qRT-PCR. The genes assayed were *acrIFI* (A); transposase, an early-expressed gene (B); *I/Z*, the scaffold gene, which lies immediately downstream of *aca1* (C); and *G*, a late gene lying directly upstream of the *acr* gene (D). Expression levels were normalized to the geometric mean of the transcript levels of two bacterial housekeeping genes: *clpX* and *rpoD*. The mean ± SEM of three independent experiments is shown. Assays were performed in PA14ΔCRISPR at a MOI of 8.

To determine whether the readthrough transcription from the strong *acr* promoter contributes to the loss of viability of the JBD30*aca1*^{R44A} phage, we inserted a single copy of the *rrnB* T1 transcriptional terminator (Orosz et al., 1991) immediately downstream of the *aca1* stop codon. Insertion of this terminator resulted in a more than 1,000-fold increase in plaquing efficiency of the JBD30*aca1*^{R44A} mutant phage (Figure S5), implying that readthrough transcription is indeed contributing to the loss of phage viability in the absence of Aca1 repressor activity. Addition of this terminator did not reduce the viability of the wild-type phage. The incomplete recovery of viability of the JBD30*aca1*^{R44A} mutant phage suggests that other factors affecting viability may also be at play or that the terminator used was not strong enough to stop readthrough transcription from the *acr* promoter.

Aca1 Can Act as an "Anti-anti-CRISPR"

Because Aca1 is a repressor of the *acr* promoter, we postulated that excessive Aca1 expression might inhibit the replication of phages requiring anti-CRISPR activity for viability in the presence of CRISPR-Cas. To test this hypothesis, we plated phage JBD30 on PA14 cells in which Aca1 was expressed from a plasmid. We found that phage replication was inhibited by more than 100-fold in the presence of plasmid-expressed Aca1 compared with cells carrying an empty vector (Figure 5A). This loss of phage replication was CRISPR-Cas-dependent because plasmid-expressed Aca1 had no effect on phage replication in the PA14ΔCRISPR strain, indicating that the impairment of phage replication results from a decrease in anti-CRISPR expression. Importantly, phages bearing mutations in IR2, which is the binding site required for Aca1-mediated repression of the *acr* promoter, were able to replicate in the presence of excess Aca1. On the other hand, a phage mutated in the IR1 site, which binds Aca1 but does not mediate repression, replicated more poorly than the wild-type in the presence of Aca1. This confirms that binding of IR2 by Aca1 is required for repression of *acr* transcription *in vivo* and indicates that, likely, IR1 titrates Aca1 away from IR2 and thereby lessens the repressive effect of Aca1. The DNA-binding activity of Aca1 is necessary to reduce JBD30 replication because overexpression of the Aca1 R44A mutant has no effect on JBD30 replication in the presence of CRISPR-Cas (Figure 5B).

Overall, the inhibitory effect of Aca1 on *acr*-dependent phage replication further bolsters our conclusion that Aca1 is a repressor of the *acr* promoter. This observation also raises the intriguing possibility that expression of Aca1 could be co-opted by bacteria as an anti-anti-CRISPR mechanism for protection against phages or other mobile genetic elements carrying anti-CRISPR genes.

Members of Other Aca Families Are Also Repressors of Anti-CRISPR Promoters

Genes encoding active anti-CRISPR proteins have been found in association with genes encoding HTH motif-containing proteins that are completely distinct in sequence from Aca1. For example, *aca2* has been found in association with five different families of anti-CRISPR genes in diverse species of Proteobacteria (Pawluk et al., 2016a, 2016b). Genes encoding homologs of Aca3, another distinctive HTH-containing protein, have been identified in association with three different type II-C anti-CRISPR genes

Please cite this article in press as: Stanley et al., Anti-CRISPR-Associated Proteins Are Crucial Repressors of Anti-CRISPR Transcription, Cell (2019), https://doi.org/10.1016/j.cell.2019.07.046

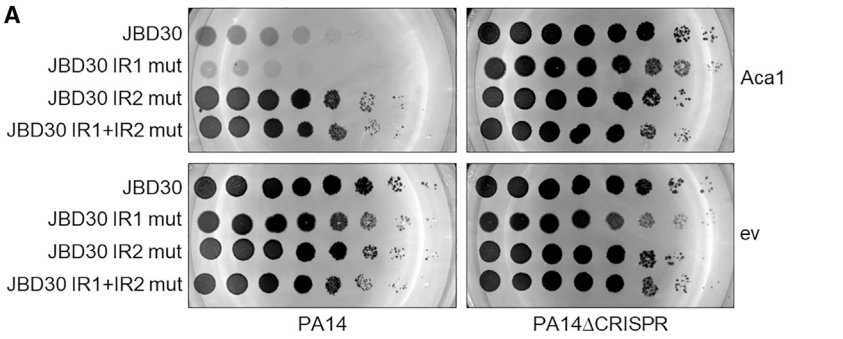

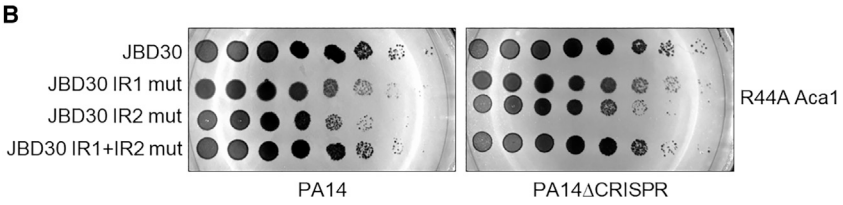

Figure 5. Overexpression of Aca1 Inhibits Phage-Borne Anti-CRISPRs

(A) 10-fold dilutions of lysates of JBD30 carrying the indicated mutations in the Aca1 binding sites (IR1 and IR2) were applied to lawns of PA14 or PA14ΔCRISPR expressing wild-type Aca1 from a plasmid. A representative image of at least three replicates is shown. (B) 10-fold dilutions of phage JBD30 lysate carrying the indicated inverted repeat mutation were applied to lawns of PA14 or PA14ΔCRISPR expressing the R44A Aca1 mutant from a plasmid. A representative image from three biological replicates is shown.

(Pawluk et al., 2016a). To investigate the generality of Aca function, we determined whether representative members of the Aca2 and Aca3 (Figures S6A and S6B) families also function as repressors of anti-CRISPR transcription.

By aligning the intergenic regions found immediately upstream of anti-CRISPR genes associated with *aca2*, we detected a conserved inverted repeat sequence that could act as a binding site for Aca2 proteins (Figure S6C). The same alignment approach also revealed an inverted repeat sequence that could act as a binding site for Aca3 (Figure S6D). To investigate the functions of Aca2 and Aca3, the *acr/aca* regions from *Pectobacterium* phage ZF40 and from *N. meningitidis* strain 2842STDY5881035 were investigated as representatives of the Aca2 and Aca3 families, respectively. The putative promoter regions of the anti-CRISPR genes in these two operons (Figures S6C and S6D) were cloned upstream of a promoterless *lacZ* reporter gene carried on a plasmid. When assayed in *E. coli*, both regions mediated robust transcription of the reporter, as detected by measuring β-galactosidase activity in cell extracts (Figure 6). Co-expression of $Aca2_{ZF40}$ and $Aca3_{Nme}$ with their putative cognate promoters resulted in 100-fold and 20-fold reductions in β-galactosidase activity, respectively. Co-expression of *aca2* with the *aca3* operon promoter construct or vice versa did not exhibit any repression, demonstrating that the repressor activities of Aca2 and Aca3 are specific to their associated promoters. Overall, these data show that, similar to Aca1, both Aca2 and Aca3 are repressors of anti-CRISPR transcription.

Anti-CRISPR Protein Is Not Packaged into Phage Particles

Although we have demonstrated that anti-CRISPRs are robustly expressed at the onset of phage infection to protect phage DNA from CRISPR-Cas-mediated degradation, additional protection would be provided if anti-CRISPR proteins were injected along with the DNA into the cell. Packaging of phage-encoded inhibitors of bacterial defense systems has been documented. For example, *E. coli* phages T4 and P1 both incorporate protein inhibitors of restriction endonucleases into their capsids and deliver them along with their genomes to protect against host defenses (Bair et al., 2007; Iida et al., 1987; Piya et al., 2017). Because these anti-restriction proteins are present at more than 40 copies per phage particle, we expected to detect anti-CRISPR protein in the phage particles if they were packaged. To assay for the presence of anti-CRISPR protein in particles of the AcrIF1-encoding phage JBD30, we performed mass spectrometry on purified phage particles. Although we were able to detect AcrIF1 in partially purified phage samples, this protein was not detected after further purification by buffer exchange, implying that AcrIF1is not incorporated into phage particles (Figures 7A and 7B). By contrast, all expected phage viral particle proteins were detected (Table S1).

For anti-CRISPR proteins to be packaged into phage particles, recognition between a virion protein and the anti-CRISPR would likely be required. This requirement has been described in other bacteriophages. For example, protein packaged into T4 particles is incorporated by a specific interaction with a core capsid scaffolding protein (Hendrix and Duda, 1998; Hong and Black, 1993), and restriction enzyme inhibitors of phage P1 are incorporated through a specific assembly pathway (Piya et al., 2017). Thus, an anti-CRISPR from one phage would not be expected to function within the context of a completely different phage. To investigate this issue, we incorporated the anti-CRISPR region of phage JBD30 (Figure 7C) into random locations in the genome of the unrelated D3-like *P. aeruginosa* phage JBD44 using transposon mutagenesis. Even though the virion proteins of JBD44 are completely unrelated to those of JBD30, the *acrIF1* region inserted into JBD44 was still able to confer resistance against the type I-F CRISPR-Cas system of PA14. The plaque-forming ability of wild-type JBD44 was robustly inhibited when targeted by the PA14 CRISPR-Cas system, whereas JBD44 phages carrying the anti-CRISPR region (JBD44::*acr*) were protected from CRISPR-Cas mediated inhibition (Figure 7D). Additionally, the level of plaquing by JBD44::*acr* phages was the same regardless of the presence or absence of a CRISPR-Cas system, suggesting that these phages exhibit full anti-CRISPR activity. These results demonstrate that AcrIF1 retains full functionality in the

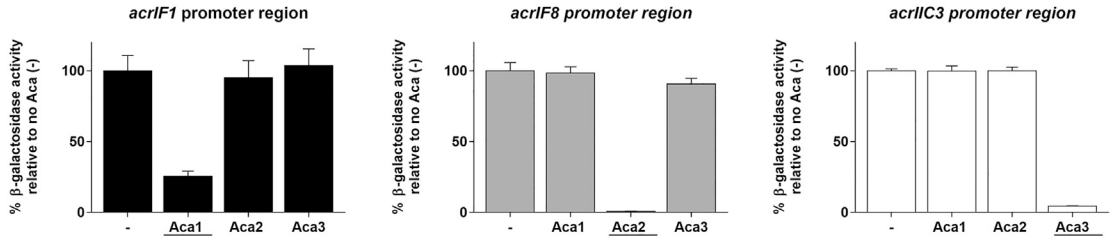

Figure 6. Members of Other Aca Families Are Repressors of Putative Anti-CRISPR Promoters

Promoter regions of *acrIF1* from *Pseudomonas* phage JBD30 and putative promoter regions of *acrIF8* from *Pectobacterium* phage ZF40 and *acrIIC3* from a *N. meningitidis* prophage were cloned upstream of a promoterless *lacZ* gene. β-Galactosidase activity was measured in the absence and presence of the indicated plasmid-expressed Aca proteins in *E. coli*. The cognate Aca for each promoter is underlined. The mean ± SEM from three biological replicates is shown. See also Figure S6.

genomic context of an entirely different phage, implying that interaction between the anti-CRISPR and other phage components (including the virion proteins) is not required. This experiment also demonstrates the transferability of *acr* operons and their ability to function in completely different genomic contexts.

DISCUSSION

Given the increasing numbers of anti-CRISPR families being discovered, we expect that they exert a strong and widespread influence on CRISPR-Cas function and have been important drivers of CRISPR-Cas evolution. The ubiquity of the association between Aca proteins and anti-CRISPRs implies that Aca proteins play a crucial role in anti-CRISPR systems; thus, an investigation into their function was timely. Here we have shown that Aca1 is a repressor of anti-CRISPR transcription and is critical for phage particle production. Because we found no evidence that AcrIF1 is incorporated into phage particles and injected into host cells along with phage DNA, our results imply that phage survival in the face of pre-formed CRISPR-Cas complexes in the host cell is dependent on rapid high-level transcription of the anti-CRISPR gene from a powerful promoter. However, the placement of such strong constitutive promoters within the context of a gene-dense, intricately regulated phage genome is likely to result in the dysregulation of critical genes and a decrease in fitness. The inclusion of repressors within anti-CRISPR operons to attenuate transcription when sufficient anti-CRISPR protein has accumulated solves this problem. We surmise that the widespread presence of *aca* genes within anti-CRISPR operons has been vital for the spread of these operons by horizontal gene transfer, allowing them to incorporate at diverse positions within phage genomes without a resulting decrease in phage viability. In addition, our work shows that Aca proteins have the potential to broadly inhibit anti-CRISPR expression, effectively acting as anti-anti-CRISPRs, which could have applications in CRISPR-based antibacterial technologies (Greene, 2018; Pursey et al., 2018).

One question with respect to anti-CRISPR operon function is how rapid high-level expression of anti-CRISPR proteins can be achieved when a repressor of the operon is produced simultaneously. Because Aca proteins are not present when phage DNA is first injected, initial transcription of anti-CRISPR operons is not impeded. In most anti-CRISPR operons, the *acr* genes precede the *aca* gene and are thus translated first, allowing anti-CRISPR proteins to accumulate earlier. In addition, the *aca* ribosome binding sites in the *aca1*-, *aca2*-, and *aca3*-controlled operons tested in this work are predicted to be considerably weaker than those of the associated *acr* genes, which would result in slower accumulation of the Aca proteins (Espah Borujeni et al., 2014; Salis et al., 2009; Seo et al., 2013). The presence of two binding sites for Aca1 in the *acr* promoter, only one of which mediates repression, may also serve to delay the repressive activity of Aca1. Evidence for this is seen in Figure 5A, where replication of a phage lacking IR1 is inhibited to a greater extent than for the wild-type by plasmid-based expression of Aca1, presumably because Aca1 is normally titrated away from the IR2 site by binding to IR1. Other mechanisms to fine-tune the balance of anti-CRISPR and Aca protein levels, such as differential protein and/or mRNA stability, may also play a role in some cases. Another notable feature of Aca1 is its weaker DNA-binding affinity compared with other well-known HTH repressors, such as the lambda, *lac*, and *tet* repressors, presumably making Aca proteins weaker repressors. This is likely a functional requirement of Aca proteins because some level of anti-CRISPR transcription is necessary for the survival of prophages, which would be targets of host CRISPR-Cas systems in the absence of anti-CRISPR activity.

In the case of phage JBD30, the absence of Aca1 function led to a dramatic increase in *acr* operon transcription and abrogation of phage particle production. This loss of viability appeared, at least in part, to result from a large decrease in the transcription of essential genes downstream of the *acr* operon (Figure 4C). We believe that this decrease is caused by readthrough transcription from the *acr* promoter, a conclusion supported by the rescue of phage viability upon insertion of a transcriptional terminator downstream of the *aca1*^{R44A} gene. In an interesting parallel, strong transcriptional readthrough from early promoters in *E. coli* phage T7 is lethal if it is not attenuated by a phage protein that inhibits *E. coli* RNA polymerase (Savalia et al., 2010). Although it seems counterintuitive that strong upstream transcription would attenuate downstream transcription, this type of transcriptional interference has been shown to result from RNA polymerase pausing over downstream promoters, dislodgement of transcription factors, or DNA supercoiling effects from high rates

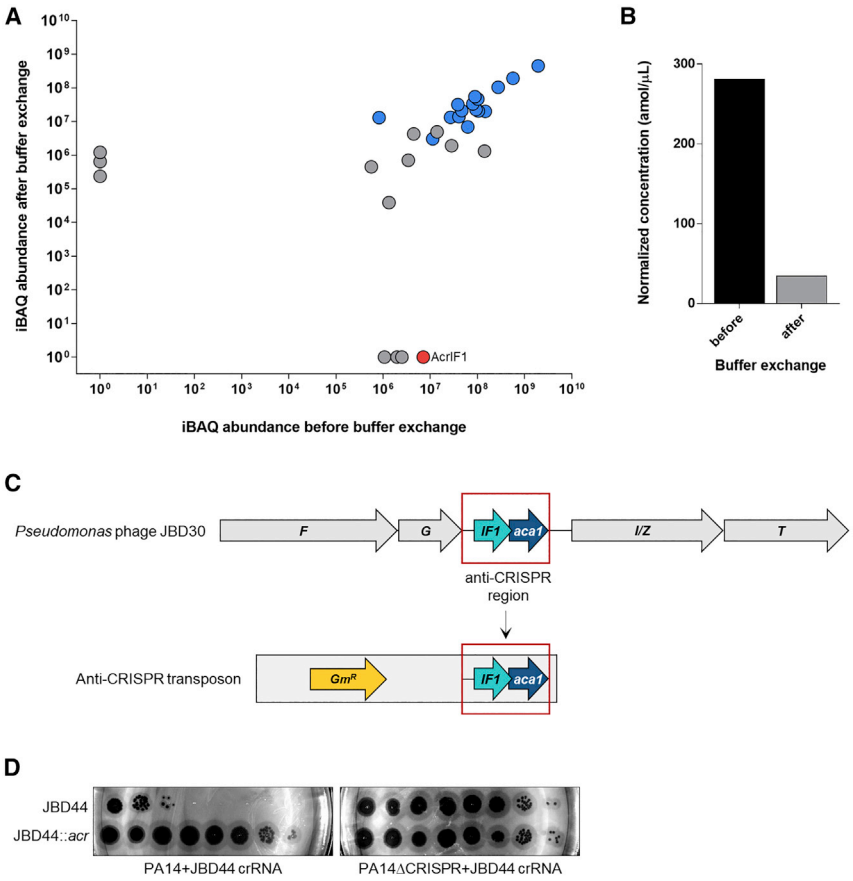

Figure 7. Anti-CRISPR AcrIF1 Is Not Incorporated into the JBD30 Virion

(A) Analysis of absolute protein abundance of phage proteins before and after buffer exchange. Phage particle proteins are highlighted in blue. AcrIFI is shown in red.

(B) Estimated concentration of AcrIF1 in phage particles before and after additional purification by buffer exchange.

(C) Schematic representation of the genomic context of AcrIF1 from phage JBD30. The anti-CRISPR region (outlined red) was inserted into a transposon, which was used to randomly introduce the anti-CRISPR region into phage JBD44. *F* and *G* encode phage head and tail morphogenesis proteins, respectively. *I/Z* encodes the protease/scaffold, and *T* encodes the major head protein.

(D) 10-fold dilutions of lysates of phage JBD44 and phage JBD44 carrying the JBD30 anti-CRISPR locus (JDB44::*acr*) were applied on lawns of PA14 and PA14ΔCRISPR expressing a crRNA targeting phage JBD44 (JBD44 crRNA) from a plasmid. A representative image of at least three biological replicates is shown.

See also Table S1.

of transcription (Hao et al., 2017; Liu and Wang, 1987; Palmer et al., 2009, 2011; Scheirer and Higgins, 2001).

Another question is why anti-CRISPR operons would include a repressor to decrease transcription rather than a strong downstream transcriptional terminator to prevent readthrough transcription. Depending on where an *acr* operon has been inserted, transcription may need to proceed through the anti-CRISPR region for essential genes to be transcribed. Thus, inserting a terminator could be detrimental. Additionally, maintaining a very high level of transcription would unnecessarily sap host resources. Consistent with this idea, highly expressed genes have generally been found to have a lower likelihood of horizontal transfer because of their greater potential to disrupt recipient physiology (Park and Zhang, 2012; Sorek et al., 2007). Our observation that terminator insertion did not completely rescue the *aca1*^{R44A} mutant also suggests that unrestrained transcription from the *acr* promoter may reduce viability through other mechanisms. In general, we expect that strong anti-CRISPR-associated promoters would reduce evolutionary fitness when placed in most locations within mobile DNA elements if these promoters were unregulated. Reductions in fitness could be due to various mechanisms of gene misregulation, depending on the specific insertional position of the *acr* operon. The great diversity of *acr* operon insertion points in mobile elements is emphasized by the distinct locations observed for nine different *acr* operons controlled by Aca2 (Figure S7A). It can be seen that the *acr* promoter/*aca* operator regions and Aca2 coding regions of these operons are remarkably conserved at the nucleotide level, whereas the Acr-encoding regions in between are highly diverse (Figure S7B), highlighting the importance of Aca regulation of the *acr* promoter.

It has been shown recently that anti-CRISPR-expressing phages like JBD30 cooperate to inhibit CRISPR-Cas systems. Initial phage infection may not result in successful phage replication, but anti-CRISPR protein accumulating from infections aborted by CRISPR-Cas activity leads to "immunosuppression" that aids in subsequent phage infections (Borges et al., 2018; Landsberger et al., 2018). By demonstrating that anti-CRISPR genes are expressed quickly after infection, we provide an explanation for how anti-CRISPR protein accumulates even when phage genomes are ultimately destroyed by the CRISPR-Cas system. In the anti-CRISPR-expressing archaeal virus SIRV2, the *acrID1* gene was also transcribed at high levels early in infection, supporting the generalizability of this mechanism of anti-CRISPR action (Quax et al., 2013).

STAR★METHODS

Detailed methods are provided in the online version of this paper and include the following:

- KEY RESOURCES TABLE
- LEAD CONTACT AND MATERIALS AVAILABILITY
- EXPERIMENTAL MODEL AND SUBJECT DETAILS
  - Microbes
  - Phages

SUPPLEMENTAL INFORMATION

Supplemental Information can be found online at https://doi.org/10.1016/j.cell.2019.07.046.

ACKNOWLEDGMENTS

The authors would like to thank Karen Maxwell, Emma Brownlie, Cayla Burk, and Véronique Taylor for useful comments on the manuscript. The authors would also like to thank Susan Kelso for help with the graphical abstract. This work was supported by NIH grants P50GM082250 and U01MH115747 (to N.J.K.) and DP5-OD021344 and R01GM127489 (to J.B.-D.) and by Canadian Institutes of Health Research grants MOP-130482 and FDN-15427 (to A.R.D.).

AUTHOR CONTRIBUTIONS

Conceptualization, S.Y.S., A.L.B., J.B.-D., and A.R.D.; Investigation, S.Y.S., A.L.B., K.-H.C., D.L.S., and J.B.-D.; Writing – Original Draft, S.Y.S. and A.R.D.; Writing – Review & Editing, S.Y.S., A.L.B., K.-H.C., D.L.S., N.J.K., J.B.-D., and A.R.D.; Supervision, D.L.S., N.J.K., J.B.-D., and A.R.D.

DECLARATION OF INTERESTS

The authors have filed for a patent related to this work.

Received: December 4, 2018
Revised: May 6, 2019
Accepted: July 25, 2019
Published: August 29, 2019

REFERENCES

Agari, Y., Sakamoto, K., Tamakoshi, M., Oshima, T., Kuramitsu, S., and Shinkai, A. (2010). Transcription profile of Thermus thermophilus CRISPR systems after phage infection. J. Mol. Biol. *395*, 270–281.

Altschul, S.F., Madden, T.L., Schäffer, A.A., Zhang, J., Zhang, Z., Miller, W., and Lipman, D.J. (1997). Gapped BLAST and PSI-BLAST: a new generation of protein database search programs. Nucleic Acids Res. *25*, 3389–3402.

Bair, C.L., Rifat, D., and Black, L.W. (2007). Exclusion of glucosyl-hydroxymethylcytosine DNA containing bacteriophages is overcome by the injected protein inhibitor IPI*. J. Mol. Biol. *366*, 779–789.

Barrangou, R., Fremaux, C., Deveau, H., Richards, M., Boyaval, P., Moineau, S., Romero, D.A., and Horvath, P. (2007). CRISPR provides acquired resistance against viruses in prokaryotes. Science *315*, 1709–1712.

Bondy-Denomy, J., Pawluk, A., Maxwell, K.L., and Davidson, A.R. (2013). Bacteriophage genes that inactivate the CRISPR/Cas bacterial immune system. Nature *493*, 429–432.

Bondy-Denomy, J., Garcia, B., Strum, S., Du, M., Rollins, M.F., Hidalgo-Reyes, Y., Wiedenheft, B., Maxwell, K.L., and Davidson, A.R. (2015). Multiple mechanisms for CRISPR-Cas inhibition by anti-CRISPR proteins. Nature *526*, 136–139.

Borges, A.L., Zhang, J.Y., Rollins, M.F., Osuna, B.A., Wiedenheft, B., and Bondy-Denomy, J. (2018). Bacteriophage Cooperation Suppresses CRISPR-Cas3 and Cas9 Immunity. Cell *174*, 917–925.e10.

Brouns, S.J., Jore, M.M., Lundgren, M., Westra, E.R., Slijkhuis, R.J., Snijders, A.P., Dickman, M.J., Makarova, K.S., Koonin, E.V., and van der Oost, J. (2008). Small CRISPR RNAs guide antiviral defense in prokaryotes. Science *321*, 960–964.

Cady, K.C., White, A.S., Hammond, J.H., Abendroth, M.D., Karthikeyan, R.S., Lalitha, P., Zegans, M.E., and O'Toole, G.A. (2011). Prevalence, conservation and functional analysis of Yersinia and Escherichia CRISPR regions in clinical Pseudomonas aeruginosa isolates. Microbiology *157*, 430–437.

Chowdhury, S., Carter, J., Rollins, M.F., Golden, S.M., Jackson, R.N., Hoffmann, C., Nosaka, L., Bondy-Denomy, J., Maxwell, K.L., Davidson, A.R., et al. (2017). Structure Reveals Mechanisms of Viral Suppressors that Intercept a CRISPR RNA-Guided Surveillance Complex. Cell *169*, 47–57e11.

Cox, J., and Mann, M. (2008). MaxQuant enables high peptide identification rates, individualized p.p.b.-range mass accuracies and proteome-wide protein quantification. Nat. Biotechnol. *26*, 1367–1372.

Cox, J., Hein, M.Y., Luber, C.A., Paron, I., Nagaraj, N., and Mann, M. (2014). Accurate proteome-wide label-free quantification by delayed normalization and maximal peptide ratio extraction, termed MaxLFQ. Mol. Cell. Proteomics *13*, 2513–2526.

Datsenko, K.A., Pougach, K., Tikhonov, A., Wanner, B.L., Severinov, K., and Semenova, E. (2012). Molecular memory of prior infections activates the CRISPR/Cas adaptive bacterial immunity system. Nat. Commun. *3*, 945.

Deltcheva, E., Chylinski, K., Sharma, C.M., Gonzales, K., Chao, Y., Pirzada, Z.A., Eckert, M.R., Vogel, J., and Charpentier, E. (2011). CRISPR RNA maturation by trans-encoded small RNA and host factor RNase III. Nature *471*, 602–607.

Dong, D., Guo, M., Wang, S., Zhu, Y., Wang, S., Xiong, Z., Yang, J., Xu, Z., and Huang, Z. (2017). Structural basis of CRISPR-SpyCas9 inhibition by an anti-CRISPR protein. Nature *546*, 436–439.

Dong, L., Guan, X., Li, N., Zhang, F., Zhu, Y., Ren, K., Yu, L., Zhou, F., Han, Z., Gao, N., and Huang, Z. (2019). An anti-CRISPR protein disables type V Cas12a by acetylation. Nat. Struct. Mol. Biol. *26*, 308–314.

Espah Borujeni, A., Channarasappa, A.S., and Salis, H.M. (2014). Translation rate is controlled by coupled trade-offs between site accessibility, selective RNA unfolding and sliding at upstream standby sites. Nucleic Acids Res. *42*, 2646–2659.

Farinha, M.A., and Kropinski, A.M. (1990). Construction of broad-host-range plasmid vectors for easy visible selection and analysis of promoters. J. Bacteriol. *172*, 3496–3499.

Garneau, J.E., Dupuis, M.E., Villion, M., Romero, D.A., Barrangou, R., Boyaval, P., Fremaux, C., Horvath, P., Magadán, A.H., and Moineau, S. (2010). The CRISPR/Cas bacterial immune system cleaves bacteriophage and plasmid DNA. Nature *468*, 67–71.

Gibson, D.G., Young, L., Chuang, R.Y., Venter, J.C., Hutchison, C.A., 3rd, and Smith, H.O. (2009). Enzymatic assembly of DNA molecules up to several hundred kilobases. Nat. Methods *6*, 343–345.

Gilbert, W., and Müller-Hill, B. (1967). The lac operator is DNA. Proc. Natl. Acad. Sci. USA *58*, 2415–2421.

Goodman, A.L., Kulasekara, B., Rietsch, A., Boyd, D., Smith, R.S., and Lory, S. (2004). A signaling network reciprocally regulates genes associated with acute

infection and chronic persistence in Pseudomonas aeruginosa. Dev. Cell *7*, 745–754.

Greene, A.C. (2018). CRISPR-Based Antibacterials: Transforming Bacterial Defense into Offense. Trends Biotechnol. *36*, 127–130.

Grenha, R., Slamti, L., Nicaise, M., Refes, Y., Lereclus, D., and Nessler, S. (2013). Structural basis for the activation mechanism of the PlcR virulence regulator by the quorum-sensing signal peptide PapR. Proc. Natl. Acad. Sci. USA *110*, 1047–1052.

Guo, T.W., Bartesaghi, A., Yang, H., Falconieri, V., Rao, P., Merk, A., Eng, E.T., Raczkowski, A.M., Fox, T., Earl, L.A., et al. (2017). Cryo-EM Structures Reveal Mechanism and Inhibition of DNA Targeting by a CRISPR-Cas Surveillance Complex. Cell *171*, 414–426.e12.

Hao, N., Palmer, A.C., Dodd, I.B., and Shearwin, K.E. (2017). Directing traffic on DNA-How transcription factors relieve or induce transcriptional interference. Transcription *8*, 120–125.

Harrington, L.B., Doxzen, K.W., Ma, E., Liu, J.J., Knott, G.J., Edraki, A., Garcia, B., Amrani, N., Chen, J.S., Cofsky, J.C., et al. (2017). A Broad-Spectrum Inhibitor of CRISPR-Cas9. Cell *170*, 1224–1233 e15.

Hendrix, R.W., and Duda, R.L. (1998). Bacteriophage HK97 head assembly: a protein ballet. Adv. Virus Res. *50*, 235–288.

Hertveldt, K., and Lavigne, R. (2008). Bacteriophages of Pseudomonas. In Pseudomonas (Wiley-VCH Verlag GmbH & Co. KGaA), pp. 255–291.

Hong, Y.R., and Black, L.W. (1993). Protein folding studies in vivo with a bacteriophage T4 expression-packaging-processing vector that delivers encapsidated fusion proteins into bacteria. Virology *194*, 481–490.

Iida, S., Streiff, M.B., Bickle, T.A., and Arber, W. (1987). Two DNA antirestriction systems of bacteriophage P1, darA, and darB: characterization of darA-phages. Virology *157*, 156–166.

Juranek, S., Eban, T., Altuvia, Y., Brown, M., Morozov, P., Tuschl, T., and Margalit, H. (2012). A genome-wide view of the expression and processing patterns of Thermus thermophilus HB8 CRISPR RNAs. RNA *18*, 783–794.

Kamionka, A., Bogdanska-Urbaniak, J., Scholz, O., and Hillen, W. (2004). Two mutations in the tetracycline repressor change the inducer anhydrotetracycline to a corepressor. Nucleic Acids Res. *32*, 842–847.

Katoh, K., Misawa, K., Kuma, K., and Miyata, T. (2002). MAFFT: a novel method for rapid multiple sequence alignment based on fast Fourier transform. Nucleic Acids Res. *30*, 3059–3066.

Knott, G.J., Thornton, B.W., Lobba, M.J., Liu, J.J., Al-Shayeb, B., Watters, K.E., and Doudna, J.A. (2019). Broad-spectrum enzymatic inhibition of CRISPR-Cas12a. Nat. Struct. Mol. Biol. *26*, 315–321.

Landsberger, M., Gandon, S., Meaden, S., Rollie, C., Chevallereau, A., Chabas, H., Buckling, A., Westra, E.R., and van Houte, S. (2018). Anti-CRISPR Phages Cooperate to Overcome CRISPR-Cas Immunity. Cell *174*, 908–916.e12.

Levy, A., Goren, M.G., Yosef, I., Auster, O., Manor, M., Amitai, G., Edgar, R., Qimron, U., and Sorek, R. (2015). CRISPR adaptation biases explain preference for acquisition of foreign DNA. Nature *520*, 505–510.

Liu, Y.C., and Matthews, K.S. (1993). Dependence of trp repressor-operator affinity, stoichiometry, and apparent cooperativity on DNA sequence and size. J. Biol. Chem. *268*, 23239–23249.

Liu, L.F., and Wang, J.C. (1987). Supercoiling of the DNA template during transcription. Proc. Natl. Acad. Sci. USA *84*, 7024–7027.

Luscombe, N.M., Austin, S.E., Berman, H.M., and Thornton, J.M. (2000). An overview of the structures of protein-DNA complexes. Genome Biol. *1*, REVIEWS001.

MacLean, B., Tomazela, D.M., Shulman, N., Chambers, M., Finney, G.L., Frewen, B., Kern, R., Tabb, D.L., Liebler, D.C., and MacCoss, M.J. (2010). Skyline: an open source document editor for creating and analyzing targeted proteomics experiments. Bioinformatics *26*, 966–968.

Makarova, K.S., Wolf, Y.I., Alkhnbashi, O.S., Costa, F., Shah, S.A., Saunders, S.J., Barrangou, R., Brouns, S.J., Charpentier, E., Haft, D.H., et al. (2015). An updated evolutionary classification of CRISPR-Cas systems. Nat. Rev. Microbiol. *13*, 722–736.

Marino, N.D., Zhang, J.Y., Borges, A.L., Sousa, A.A., Leon, L.M., Rauch, B.J., Walton, R.T., Berry, J.D., Joung, J.K., Kleinstiver, B.P., and Bondy-Denomy, J. (2018). Discovery of widespread type I and type V CRISPR-Cas inhibitors. Science *362*, 240–242.

Marraffini, L.A., and Sontheimer, E.J. (2008). CRISPR interference limits horizontal gene transfer in staphylococci by targeting DNA. Science *322*, 1843–1845.

Marrs, C.F., and Howe, M.M. (1990). Kinetics and regulation of transcription of bacteriophage Mu. Virology *174*, 192–203.

Nelson, H.C., and Sauer, R.T. (1985). Lambda repressor mutations that increase the affinity and specificity of operator binding. Cell *42*, 549–558.

Orosz, A., Boros, I., and Venetianer, P. (1991). Analysis of the complex transcription termination region of the Escherichia coli rrnB gene. Eur. J. Biochem. *201*, 653–659.

Palmer, A.C., Ahlgren-Berg, A., Egan, J.B., Dodd, I.B., and Shearwin, K.E. (2009). Potent transcriptional interference by pausing of RNA polymerases over a downstream promoter. Mol. Cell *34*, 545–555.

Palmer, A.C., Egan, J.B., and Shearwin, K.E. (2011). Transcriptional interference by RNA polymerase pausing and dislodgement of transcription factors. Transcription *2*, 9–14.

Park, C., and Zhang, J. (2012). High expression hampers horizontal gene transfer. Genome Biol. Evol. *4*, 523–532.

Pawluk, A., Amrani, N., Zhang, Y., Garcia, B., Hidalgo-Reyes, Y., Lee, J., Edraki, A., Shah, M., Sontheimer, E.J., Maxwell, K.L., et al. (2016a). Naturally Occurring Off-Switches for CRISPR-Cas9. Cell *167*, 1829–1838.e9.

Pawluk, A., Staals, R.H., Taylor, C., Watson, B.N., Saha, S., Fineran, P.C., Maxwell, K.L., and Davidson, A.R. (2016b). Inactivation of CRISPR-Cas systems by anti-CRISPR proteins in diverse bacterial species. Nat. Microbiol. *1*, 16085.

Pawluk, A., Shah, M., Mejdani, M., Calmettes, C., Moraes, T.F., Davidson, A.R., and Maxwell, K.L. (2017). Disabling a Type I-E CRISPR-Cas Nuclease with a Bacteriophage-Encoded Anti-CRISPR Protein. MBio *8*, e01751-17.

Piya, D., Vara, L., Russell, W.K., Young, R., and Gill, J.J. (2017). The multicomponent antirestriction system of phage P1 is linked to capsid morphogenesis. Mol. Microbiol. *105*, 399–412.

Pursey, E., Sünderhauf, D., Gaze, W.H., Westra, E.R., and van Houte, S. (2018). CRISPR-Cas antimicrobials: Challenges and future prospects. PLoS Pathog. *14*, e1006990.

Quax, T.E., Voet, M., Sismeiro, O., Dillies, M.A., Jagla, B., Coppée, J.Y., Sezonov, G., Forterre, P., van der Oost, J., Lavigne, R., and Prangishvili, D. (2013). Massive activation of archaeal defense genes during viral infection. J. Virol. *87*, 8419–8428.

Salis, H.M., Mirsky, E.A., and Voigt, C.A. (2009). Automated design of synthetic ribosome binding sites to control protein expression. Nat. Biotechnol. *27*, 946–950.

Sambrook, J., and Russell, D.W. (2006). Purification of Bacteriophage lambda Particles by Isopycnic Centrifugation through CsCl Gradients. CSH Protoc *2006*, pdb.prot3968.

Savalia, D., Robins, W., Nechaev, S., Molineux, I., and Severinov, K. (2010). The role of the T7 Gp2 inhibitor of host RNA polymerase in phage development. J. Mol. Biol. *402*, 118–126.

Scheirer, K.E., and Higgins, N.P. (2001). Transcription induces a supercoil domain barrier in bacteriophage Mu. Biochimie *83*, 155–159.

Schneider, C.A., Rasband, W.S., and Eliceiri, K.W. (2012). NIH Image to ImageJ: 25 years of image analysis. Nat. Methods *9*, 671–675.

Schwanhäusser, B., Busse, D., Li, N., Dittmar, G., Schuchhardt, J., Wolf, J., Chen, W., and Selbach, M. (2011). Global quantification of mammalian gene expression control. Nature *473*, 337–342.

Seo, S.W., Yang, J.S., Kim, I., Yang, J., Min, B.E., Kim, S., and Jung, G.Y. (2013). Predictive design of mRNA translation initiation region to control prokaryotic translation efficiency. Metab. Eng. *15*, 67–74.

Shanks, R.M., Caiazza, N.C., Hinsa, S.M., Toutain, C.M., and O'Toole, G.A. (2006). Saccharomyces cerevisiae-based molecular tool kit for manipulation of genes from gram-negative bacteria. Appl. Environ. Microbiol. *72*, 5027–5036.

Sievers, F., Wilm, A., Dineen, D., Gibson, T.J., Karplus, K., Li, W., Lopez, R., McWilliam, H., Remmert, M., Söding, J., et al. (2011). Fast, scalable generation of high-quality protein multiple sequence alignments using Clustal Omega. Mol. Syst. Biol. *7*, 539.

Söding, J., Biegert, A., and Lupas, A.N. (2005). The HHpred interactive server for protein homology detection and structure prediction. Nucleic Acids Res. *33*, W244-8.

Solovyev, V., and Salamov, A. (2011). Automatic Annotation of Microbial Genomes and Metagenomic Sequences. In Metagenomics and its applications in agriculture, biomedicine, and environmental studies, R.W. Li, ed. (New York: Nova Science), pp. 61–78.

Sorek, R., Zhu, Y., Creevey, C.J., Francino, M.P., Bork, P., and Rubin, E.M. (2007). Genome-wide experimental determination of barriers to horizontal gene transfer. Science *318*, 1449–1452.

Wang, X., Yao, D., Xu, J.G., Li, A.R., Xu, J., Fu, P., Zhou, Y., and Zhu, Y. (2016). Structural basis of Cas3 inhibition by the bacteriophage protein AcrF3. Nat. Struct. Mol. Biol. *23*, 868–870.

Yosef, I., Goren, M.G., and Qimron, U. (2012). Proteins and DNA elements essential for the CRISPR adaptation process in Escherichia coli. Nucleic Acids Res. *40*, 5569–5576.

Young, J.C., Dill, B.D., Pan, C., Hettich, R.L., Banfield, J.F., Shah, M., Fremaux, C., Horvath, P., Barrangou, R., and Verberkmoes, N.C. (2012). Phage-induced expression of CRISPR-associated proteins is revealed by shotgun proteomics in Streptococcus thermophilus. PLoS ONE *7*, e38077.

Zhang, X., and Bremer, H. (1995). Control of the Escherichia coli rrnB P1 promoter strength by ppGpp. J. Biol. Chem. *270*, 11181–11189.

STAR★METHODS

KEY RESOURCES TABLE

REAGENT or RESOURCE	SOURCE	IDENTIFIER
Bacterial and Virus Strains		
Pseudomonas aeruginosa strain UCBPP-PA14	A. Davidson Lab	Refseq: NC_008463.1
Pseudomonas aeruginosa strain UCBPP-PA14 Δ*cas* (PA14ΔCRISPR)	G. O'Toole Lab	N/A
Pseudomonas phage JBD30	A. Davidson Lab	Refseq: NC_020198.1
Pseudomonas phage JBD30*acr*$_{fs}$	A. Davidson Lab	N/A
Pseudomonas phage JBD30Δ*Pacr*	This paper	N/A
Pseudomonas phage JBD30 IR1 mut	This paper	N/A
Pseudomonas phage JBD30 IR2 mut	This paper	N/A
Pseudomonas phage JBD30 IR1+IR2 mut	This paper	N/A
Pseudomonas phage JBD30*aca1*^{R33A}	This paper	N/A
Pseudomonas phage JBD30*aca1*^{R34A}	This paper	N/A
Pseudomonas phage JBD30*aca1*$^{R33A/R34A}$	This paper	N/A
Pseudomonas phage JBD30*aca1*^{R44A}	This paper	N/A
Pseudomonas phage JBD30*aca1*^{R44A} IR1+IR2 mut	This paper	N/A
Pseudomonas phage JBD30*aca1*^{R44A}+*rrnB* T1	This paper	N/A
Pseudomonas phage JBD44	A. Davidson Lab	Refseq: NC_030929.1
Pseudomonas phage JBD44::*acr*	This paper	N/A
Escherichia coli DH5α	A. Davidson Lab	N/A
Escherichia coli BL21(DE3)	A. Davidson Lab	N/A
Escherichia coli SM10 λpir	K. Maxwell Lab	N/A
Chemicals, Peptides, and Recombinant Proteins		
Acid phenol:chloroform	Ambion	Cat#AM9722
Ni-NTA agarose resin	QIAGEN	Cat#30210
SYBR Gold nucleic acid stain	Invitrogen	Cat#S11494
Purified protein: Aca1, AcrIFI	This paper	N/A
Critical Commercial Assays		
TURBO DNA-free kit	Ambion	Cat#AM1907
SuperScript IV VILO master mix	Invitrogen	Cat#11754050
PowerUp SYBR Green master mix	Applied Biosystems	Cat#A25741
In-Fusion HD cloning kit	Clonetech	Cat#638912
Phusion High-Fidelity DNA Polymerase	Thermo Scientific	Cat#F530S
Oligonucleotides		
For cloning, RT-qPCR, and EMSA	This paper	See Table S4
crRNA targeting JBD44: GGTTCACTGCCGTATAGGC AGCTAAGAAAAGTTCCTTTCCCTTCAGTCCAGCCT GTGCCAGGTTCACTGCCGTGTAGGCAGCTAAGAAA	This paper	N/A
Recombinant DNA		
pHERD30T (gent^{R})	A. Davidson Lab	GenBank: EU603326.1
pHERD30T derivatives	This paper	See Table S5
pHERD20T (amp^{R})	A. Davidson Lab	GenBank: EU603324.1
pHERD20T derivatives	This paper	See Table S5
pBTK30	S. Lorry Lab	N/A
pBTK30 derivatives	This paper	See Table S5

(*Continued on next page*)

Continued

REAGENT or RESOURCE	SOURCE	IDENTIFIER
pCM-Str	J. Nodwell Lab	N/A
pCM-Str derivatives	This paper	See Table S5
pQF50	A. Davidson Lab	N/A
pQF50 derivatives	This paper	See Table S5
p15TV-L	Addgene	ID #26093
Software and Algorithms		
Prism 7.0	GraphPad	https://www.graphpad.com/scientific-software/prism
Image Lab 6.0	BioRad	http://www.bio-rad.com/en-ca/product/image-lab-software
ImageJ	NIH	https://imagej.nih.gov/ij/index.html
PyMol	Schrödinger	http://www.pymol.org
MaxQuant	Cox and Mann, 2008	http://www.coxdocs.org/doku.php?id = :maxquant:start
Skyline	MacLean et al., 2010	https://skyline.ms/project/home/software/Skyline/begin.view?
Jalview	Jalview	http://www.jalview.org
CFX Manager 3.1	BioRad	http://www.bio-rad.com/en-ca/product/cfx-manager-software
Other		
CFX384 Touch Real-Time PCR Detection System	BioRad	Cat#1855485
gBlocks for cloning of *aca2*, *aca3*, and associated promoter regions	This paper	See Table S6

LEAD CONTACT AND MATERIALS AVAILABILITY

Further information and requests for resources and reagents should be directed to and will be fulfilled by the Lead Contact, Alan R. Davidson (alan.davidson@utoronto.ca).

EXPERIMENTAL MODEL AND SUBJECT DETAILS

Microbes

Pseudomonas aeruginosa strains (UCBPP-PA14 and UCBPP-PA14 CRISPR mutant derivatives) and *Escherichia coli* strains (DH5α, SM10λpir, BL21(DE3)) were cultured at 37°C in lysogeny broth (LB) or on LB agar supplemented with antibiotics at the following concentrations when appropriate: ampicillin, 100 μg mL^{-1} for *E. coli*; carbenicillin, 300 μg mL^{-1} for *P. aeruginosa*; gentamicin, 30 μg mL^{-1} for *E. coli* and 50 μg mL^{-1} for *P. aeruginosa*.

Phages

Pseudomonas aeruginosa phages JBD44, JBD30 and JBD30 derivatives, DMS3 and DMS3 derivatives were propagated on PA14Δ CRISPR and stored in SM buffer (100 mM NaCl, 8 mM Mg_2SO4, 50 mM Tris-HCl pH 7.5, 0.01% w/v gelatin) over chloroform at 4°C.

METHOD DETAILS

Phage plaque and spotting assays

For spotting assays, 150 μL of overnight culture was added to 4 mL of molten top agar (0.7%) supplemented with 10 mM $MgSO_4$ and poured over prewarmed LB agar plates containing 10 mM $MgSO_4$ and antibiotic as needed. After solidification of the top agar lawn, 10-fold serial dilutions of phage lysate were spotted on the surface. The plates were incubated upright overnight at 30°C.

For plaque assays, 150 μL of overnight culture was mixed with an appropriate amount of phage and incubated at 37°C for 10 minutes. The bacteria/phage mixture was added to 4 mL of molten top agar (0.7%) supplemented with 10 mM $MgSO_4$ and poured over prewarmed LB agar plates containing 10 mM $MgSO_4$ and antibiotic as needed. The plates were incubated upright overnight at 30°C. Plaques were counted and expressed as the number of plaque forming units (PFU) mL^{-1}. Plaque sizes were analyzed using

ImageJ (Schneider et al., 2012). Images of plaque assays were converted to 8-bit (greyscale). The image threshold was then adjusted to isolate plaques from the image background. The area of each plaque was measured in pixels squared. Image sizes were calibrated using the diameter of the Petri dish in the image.

Phage infection time course

Overnight cultures of PA14 or PA14ΔCRISPR were subcultured 1:100 into LB and grown with shaking at 37°C to an OD_{600} of 0.4. After removing 1 mL of culture for an uninfected control, phage JBD30 was added at a multiplicity of infection (MOI) of 5 or 8. Samples were removed after 0, 2, 4, 6, 8, 10, 20, 30, 40, 50, 60, and 70 minutes. Cells were pelleted and flash frozen. One round of infection was stopped at 70 minutes post phage addition. To help synchronize the infection, cells were pelleted 10 minutes post phage addition and resuspended in fresh pre-warmed LB.

Lysogens were subcultured 1:100 from overnight cultures and grown for 5 hours prior to RNA extraction.

RNA extraction and RT-qPCR

Cell pellets were resuspended in 800 μL LB and mixed with 100 μL lysis buffer (40 mM sodium acetate, 1% SDS, 16 mM EDTA) and 700 μL acid phenol:chloroform pre-heated at 65°C. The mixture was incubated at 65°C for 5 minutes with regular vortexing and centrifuged at 12,000 x *g* for 10 minutes at 4°C. The aqueous layer was collected, extracted with chloroform, and precipitated with ethanol. Total RNA was resuspended in water and subsequently treated with DNase (TURBO DNA-free kit, Ambion) according to the manufacturer's instructions. cDNA was synthesized using SuperScript IV VILO master mix (Invitrogen) and quantified using PowerUp SYBR Green master mix (Applied Biosystems) with primers listed in Table S4. For the purpose of quantification, standards were generated by PCR. Data were analyzed using BioRad CFX manager 3.1 software.

aca gene and promoter region cloning

aca1 and its associated promoter region were PCR amplified from lysates of phage JBD30 using the primers listed in Table S4. *aca1* was cloned as a NcoI/HindIII restriction fragment into pHERD30T (for anti-CRISPR activity assays in *P. aeruginosa*) or into BseR1/HindIII cut p15TV-L (for protein expression and purification in *E.* coli with an N-terminal His_6 tag). The promoter region was cloned as a NcoI/HindIII restriction fragment into the promoterless β-galactosidase reporter shuttle vector pQF50 (Farinha and Kropinski, 1990).

The anti-CRISPR locus from *Pectobacterium* phage ZF40 (NC_019522.1: 19220-19999) and the anti-CRISPR upstream region and Aca3 coding sequence from *Neisseria meningitidis* strain 2842STDY5881035 (NZ_FERW01000005.1: 56624-56978; NZ_FERW01000005.1*:* 55654- 55893) were synthesized as gBlocks (Integrated DNA Technologies). *aca2* and *aca3* were PCR amplified from their respective gBlocks using primers list in Table S4. Each fragment was gel purified and cloned into pCM-Str using isothermal assembly (Gibson et al., 2009). The anti-CRISPR upstream regions from ZF40 and *N. meningitidis* were amplified by PCR and cloned as a NcoI/HindIII restriction fragment into pQF50. All plasmids were verified by sequencing.

β-Galactosidase reporter assays

β-Galactosidase reporter plasmids were transformed into DH5α and PA14. Overnight cultures of transformed cells were subcultured 1:100 and grown for ~3 hours with shaking (OD_{600} = 0.4-0.7). β-Galactosidase activity was then quantified using a method derived from Zhang and Bremer (1995). Briefly, 20 μL of culture was mixed with 80 μL of permeabilization solution (0.8 mg mL^{-1} CTAB, 0.4 mg mL^{-1} sodium deoxycholate, 100 mM Na_2HPO_4, 20 mM KCl, 2 mM $MgSO_4$, 5.4 μL mL^{-1} β- mercaptoethanol) and incubated at 30°C for 30 minutes. 600 μl of substrate solution (60 mM Na_2HPO_4, 40 mM NaH_2PO_4, 1 mg mL^{-1} o-nitrophenyl-β-galactosidase) was added and the reaction was allowed to proceed at 30°C for 30 minutes to 1.5 hours. The reaction was stopped with the addition of 700 μL of 1 M Na_2CO_3, A_{420} and A_{550} were measured, and Miller Units were calculated.

Aca1 amino acid substitutions

Key residues of the Aca1 HTH domain were identified using HHpred and modeled onto the HTH domain of PlcR (PDB: 3U3W) using PyMol to generate a reference homology model of Aca1. Alanine substitutions at key Aca1 residues were introduced by site-directed mutagenesis with Phusion polymerase (Thermo Scientific) in either pHERD30T (for *P. aeruginosa* activity assays) or p15TV-L (for protein expression and purification in *E. coli*).

Purification of AcrIF1 and Aca1 proteins

Overnight cultures of *E. coli* BL21(DE3) carrying the appropriate AcrIF1 or Aca1 expression plasmid were subcultured 1:100 and grown with shaking at 37°C to an OD_{600} of 0.5. Protein expression was induced with 1 mM IPTG for 4 hours at 37°C. Cells were lysed by sonication in binding buffer (20 mM Tris-HCl pH 7.5, 250 mM NaCl, 5 mM imidazole). Clarified lysates were batch bound to Ni-NTA agarose resin (QIAGEN) at 4°C for 1 hour, passed through a column at room temperature, and washed extensively with binding buffer containing 30 mM imidazole. Bound protein was eluted with binding buffer containing 250 mM imidazole and dialyzed overnight at 4°C in buffer containing 10 mM Tris-HCl pH 7.5 and 150 mM NaCl. All Aca1 mutant purified at levels similar to wild-type. Proteins were purified to greater than 95% homogeneity as assessed by Coomassie-stained SDS-PAGE.

Electrophoretic mobility shift assay

Varying concentrations of purified Aca1 or Aca1 mutants were mixed with 20 ng of target DNA (gel purified PCR product or annealed oligo) in binding buffer (10 mM HEPES pH 7.5, 1 mM $MgCl_2$, 20 mM KCl, 1 mM TCEP, 6% v/v glycerol; final reaction volume 20 μL) and incubated on ice for 20 minutes. The DNA-protein complexes were separated by gel electrophoresis at 100 V on a 6% native 0.5X TBE polyacrylamide gel. Gels were stained at room temperature with SYBR Gold (Invitrogen) and visualized according to the supplier's instructions. Bands were quantified using Image Lab 6.0 software (BioRad). The percent DNA bound was plotted as a function of Aca1 concentration in Prism 7.0 (GraphPad).

Annealed oligos were generated by mixing complementary oligonucleotides in a 1:1 molar ratio in annealing buffer (10 mM Tris, pH 7.5, 50 mM NaCl, 1 mM EDTA), heating at 95°C for 5 minutes, and cooling slowly to room temperature.

Operator and Aca1 mutant phage construction

Point mutations were introduced into each inverted repeat of the *acr* promoter on a recombination cassette (JBD30 genes 34 to 38; Bondy-Denomy et al., 2013) by site-directed mutagenesis using primers listed in Table S4. Alanine substitutes of key Aca1 residues were introduced into the wild-type JBD30 recombination cassette by site-directed mutagenesis. Mutant phages were then generated using *in vivo* recombination as previously described by Bondy-Denomy et al. (2013). All mutations were verified by sequencing.

Anti-CRISPR promoter deletion in phage JBD30

A recombination cassette consisting of genes 34 to 38 of phage JBD30 (anti-CRISPR locus with large flanking regions) in plasmid pHERD20T was previously generated (Bondy-Denomy et al., 2013). This plasmid was linearized by PCR using primers that excluded the *acr* promoter, and then re-circularized using In-fusion HD technology (Clontech) to generate a recombination cassette with an *acr* promoter deletion. Using this cassette, mutant phages were generated as previously described (Bondy-Denomy et al., 2013).

Terminator insertion into phage JBD30

The *rrnB* T1 terminator from plasmid pMQ70 (GenBank: DQ642035.1; Shanks et al., 2006) was PCR amplified using primers listed in Table S4 and inserted into the JBD30 gene 34 to 38 recombination cassette in pHERD20T by isothermal assembly (Gibson et al., 2009). Terminator insertion phages were generated by i*n vivo* recombination as previously described (Bondy-Denomy et al., 2013)

Lysogen construction

P. aeruginosa lysogens were generated by either streaking out cells to single colonies from the center of a phage-induced zone of clearing or by plating cells infected with phage and isolating single colonies. The presence of a prophage was confirmed by resistance to superinfection from the phage used to generate the lysogen.

Bioinformatics

Protein sequence similarity searches were performed with PSI-BLAST (Altschul et al., 1997). Protein sequence alignments were performed with MAFFT (Katoh et al., 2002), and nucleotide sequence alignments were performed with ClustalO (Sievers et al., 2011). HHpred was used to predict the location of HTH motifs (Söding et al., 2005).

Mass spectrometry of the JBD30 virion

Phage particles were purified from lysates by two sequential rounds of cesium chloride density gradient ultracentrifugation (Sambrook and Russell, 2006). Following ultracentrifugation, further purification was achieved by buffer exchange into gelatin-free SM using a 100 kDa MWCO centrifugal filter unit (MilliporeSigma). For mass spectrometry experiments, Ni-NTA affinity purified AcrIF1 was further purified by size exclusion chromatography as previously described (Bondy-Denomy et al., 2015).

For mass spectrometry, phage particles were sonicated in SM buffer without gelatin on ice. All samples (phage particles or purified AcrIF1 protein) were reduced in 10 mM dithiothreitol for 30 minutes at room temperature in the dark, then alkylated with 10 mM of iodoacetamide for 30 minutes at room temperature in the dark. The total protein concentration of the phage particles was determined by Bradford assay. Samples were digested with trypsin (Promega) at a 1:100 enzyme:substrate ratio at 37°C overnight. Following digestion, samples were acidified with addition of 10% trifluoroacetic acid and desalted on MiniSpin C18 tips (The Nest Group). The eluates were then dried by SpeedVac, and resuspended in 4% formic acid, 2% acetonitrile in water for MS analysis. For AcrIF1, a standard curve with protein concentrations of 0.05, 0.1, 0.2, 0.5, 0.75, 1, 2, and 5 fmol μL^{-1} was prepared. Samples were then analyzed by liquid chromatography tandem-mass spectrometry on a Q-Exactive Plus (Thermo Fisher) mass spectrometer equipped with an EASY-nLC 1200 system (Thermo Fisher). Peptides were loaded on a 75 μm ID column packed with 25 cm of Reprosil C18 1.9 μm, 120 Å particles (Dr. Maisch GmbH). The compositions of mobile phase A and B were 0.1% formic acid in water and 0.1% formic acid in 80% acetonitrile, respectively. Digested peptide mixtures were separating from 1 to 56 minutes with 4% to 22% B over a 75 minute gradient at a flow rate of 300 nL $minute^{-1}$.

Purified phage particle peptides were analyzed via a discovery-based acquisition method (data-dependent acquisition, DDA) to estimate their absolute abundance using the iBAQ calculation (Schwanhäusser et al., 2011) in the MaxQuant program (Cox et al., 2014; Cox and Mann, 2008). DDA spectra were searched against AcrIF1 sequence and JBD30 protein databases.

The phage particles as well as purified AcrIF1 were also analyzed via a parallel reaction monitoring (PRM) targeted proteomic approach of only the AcrIF1 protein. Quantitation of AcrIF1 was based on the fragmentation of the precursor peptide VENVVNGK ion 429.7376++ m/z to the product ions [y3] 318.1772+, [y4] 417.2456+, and [y7] 759.3995+ m/z found to be the most analytically robust. All three transition ion peak area intensities were integrated and summed for quantitation. All PRM data was analyzed with Skyline (MacLean et al., 2010).

PRM targets for AcrIF1

Analyte	Isolation m/z	Transition m/z
VENVVNGK	429.737617	429.737617++ to [y7] 759.399543+, 429.737617++ to [y4] 417.245609+, 429.737617++ to [y3] 318.177195+
IENAMNEISR	588.787512	588.787512++ to [y8] 934.441091+, 588.787512++ to [y7] 820.398163+, 588.787512++ to [y6] 749.361049+, 588.787512++ to [y5] 618.320565+

Anti-CRISPR locus introduction into JBD44

The anti-CRISPR locus of phage JBD30 was PCR amplified and cloned as a SalI restriction fragment into the transposon of pBTK30 (Goodman et al., 2004). This construct was transformed into *E. coli* SM10λpir. Conjugation was then used to move the transposon into a JBD44 lysogen of PA14. Following conjugation, lysogens were grown to log phase (OD_{600} = 0.5) and prophages were induced with mitomycin C (3 μg mL^{-1}). Lysates were plated on lawns of PA14 expressing a crRNA targeting phage JBD44 from pHERD30T to isolate phages carrying and expressing the anti-CRISPR locus.

Aca3 misannotation

A nucleotide alignment of several anti-CRISPR loci from *Neisseria meningitidis* revealed that many *aca3* homologs had one to two in-frame start codons (ATG) upstream of their annotated start that would result in a N-terminal extension of 8 to 10 amino acid residues. *aca3* was cloned with and without this N-terminal extension. Aca3 repressor activity was best with the inclusion of the N-terminal extension (sequence shown below with new residues in bold). Thus, this version was used in all experiments presented here. All other Aca protein sequences are as annotated.

Aca3**: MKMRRIWRAG**MIDNPELGYTPANLKAIRQKYGLTQKQVADITGATLSTAQKWE
AAMSLKTHSDMPHTRWL LLLEYVRNL

QUANTIFICATION AND STATISTICAL ANALYSIS

All experiments were performed with at least three biological replicates ($n \geq 3$). Statistical parameters are reported in the Figure Legends.

DATA AND CODE AVAILABILITY

This study did not generate/analyze any datasets/codes.

Cell

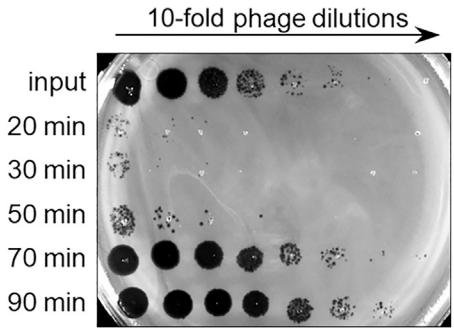

Figure S1. Infection Time Course of Phage JBD30, Related to Figures 2A and 4

10-fold dilutions of phage samples collected through the course of phage infection in wild-type PA14 were applied to lawns of wild-type PA14. Phages and cells were mixed at time = 0. The "input" is the phage titer immediately after phage addition. This number decreases by 20 minutes as all the added phages have adsorbed to cells, but new particles have not yet been produced. During the first 50 minutes after infection, few phages are produced while the full phage burst appears to have occurred by 70 minutes.

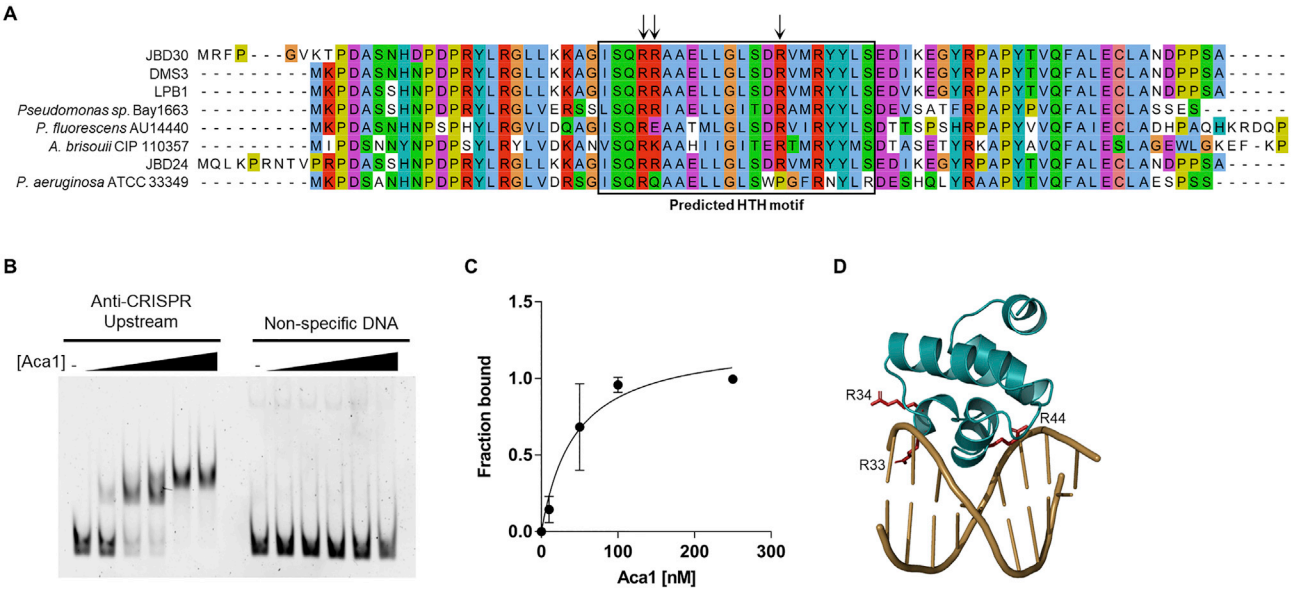

Figure S2. Bioinformatic and Functional Analysis of Aca1, Related to Figures 2 and 3

(A) Multiple sequence alignment of Aca1 homologs from the indicated phages and bacteria. The position of the predicted HTH motif is outlined in a black box. Arrows indicate R33, R34, and R44 that were subject to alanine substitution. (B) Representative EMSA with Aca1 using the 110 bp anti-CRISPR upstream region from phage JBD30 as a substrate. Purified protein was added at concentrations of 10 nM, 50 nM, 100 nM, 250 nM and 500 nM. The dash sign (-) indicates that no protein was added. Non-denaturing acrylamide gels stained with SYBR Gold are shown. (C) Quantification of DNA bound by Aca1 in EMSAs. Error bars represent the standard deviation of the mean of three replicates. (D) To indicate their position relative to a DNA substrate, residues R33, R34, and R44 (highlighted in red) of JBD30 Aca1 were modeled onto the HTH DNA-binding domain of the virulence regulator PlcR in complex with DNA (PDB: 3U3W) from *Bacillus thuringiensis* (Grenha et al., 2013).

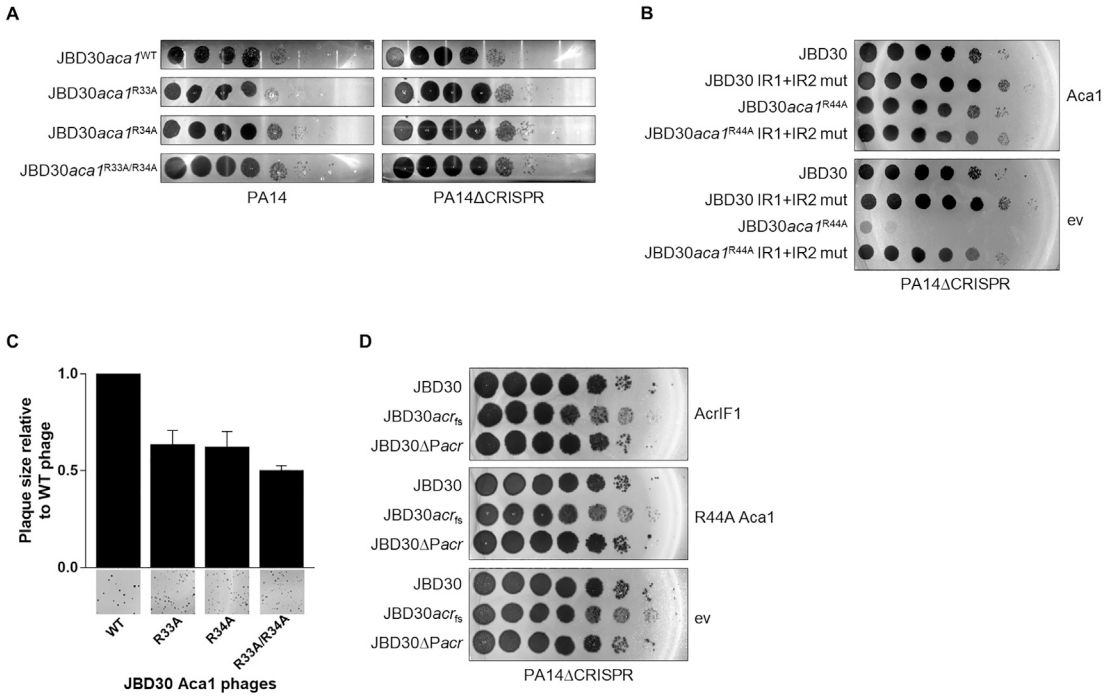

Figure S3. Effect of Aca1 Mutations and Overexpression on Phage Viability, Related to Figure 3

(A) 10-fold dilutions of lysates of the JBD30 phage carrying the indicated Aca1 mutation were applied to lawns of PA14 and PA14ΔCRISPR. A representative image from three biological replicates is shown. (B) 10-fold dilutions of lysates of JBD30 carrying the indicated mutations in Aca1 binding sites and/or Aca1 were applied to lawns of PA14ΔCRISPR overexpressing wild-type Aca1 from a plasmid. (C) The plaque sizes (area) of the Aca1 partial DNA binding mutants in phage JBD30 were quantified on the PA14ΔCRISPR strain. The average size is shown relative to that of wild-type JB30 phage. Averages were calculated from three independent plaque assays, where > 100 plaques were measured. Error bars represent the standard error of the mean. Representative plaque images are shown. (D) 10-fold dilutions of wild-type (JBD30), anti-CRISPR gene frameshift mutant (JBD30acr_{fs}) phage, and *acr* promoter deletion phage (JBD30ΔP*acr*) lysates were applied to lawns PA14ΔCRISPR overexpressing AcrIF1 and R44A Aca1 from their native promoter on a plasmid.

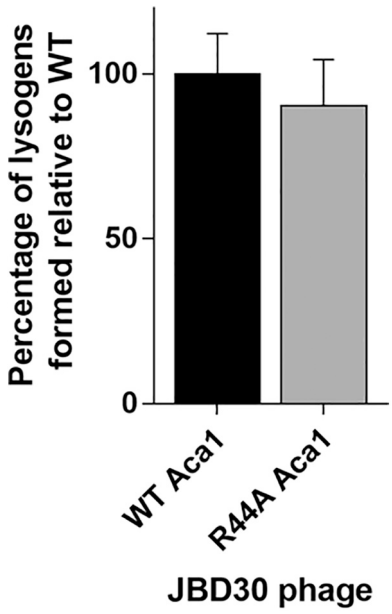

Figure S4. Phage JBD30 Lysogen Formation Is Unaffected by the R44A Aca1 Substitution, Related to Figure 4

The PA14ΔCRISPR strain was infected with wild-type JBD30 (WT Aca1) or JBD30*aca1*^{R44A} (R44A Aca1) at the same MOI and plated to single colonies. Lysogens were identified by cross-streaking the colonies over top of a line of phage lysate. The mean ± SEM percentage of lysogens formed in three independent infection assays where 100 colonies were screened relative to the wild-type phage is shown.

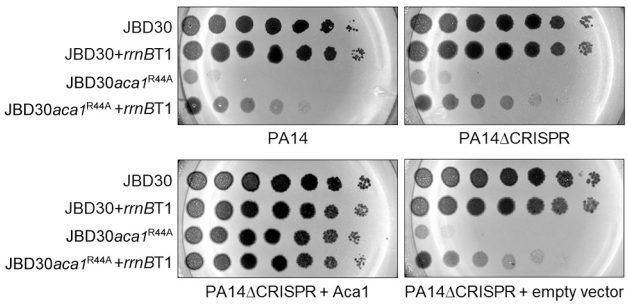

Figure S5. Insertion of a Transcriptional Terminator Downstream of the Anti-CRISPR Operon Partially Rescues JBD30*aca1*^{R44A} Viability, Related to Figure 4

Lysates of phage JBD30 (WT or Aca1 R44A mutant) with or without an inserted *rrnB* T1 terminator downstream of *aca1* were spotted in 10-fold serial dilutions on lawns of wild-type *P. aeruginosa* PA14, a CRISPR deletion strain of PA14 (PA14ΔCRISPR), or on the deletion strain expressing Aca1 from a plasmid. Representative images from three biological replicates incubated for 42 hours are shown.

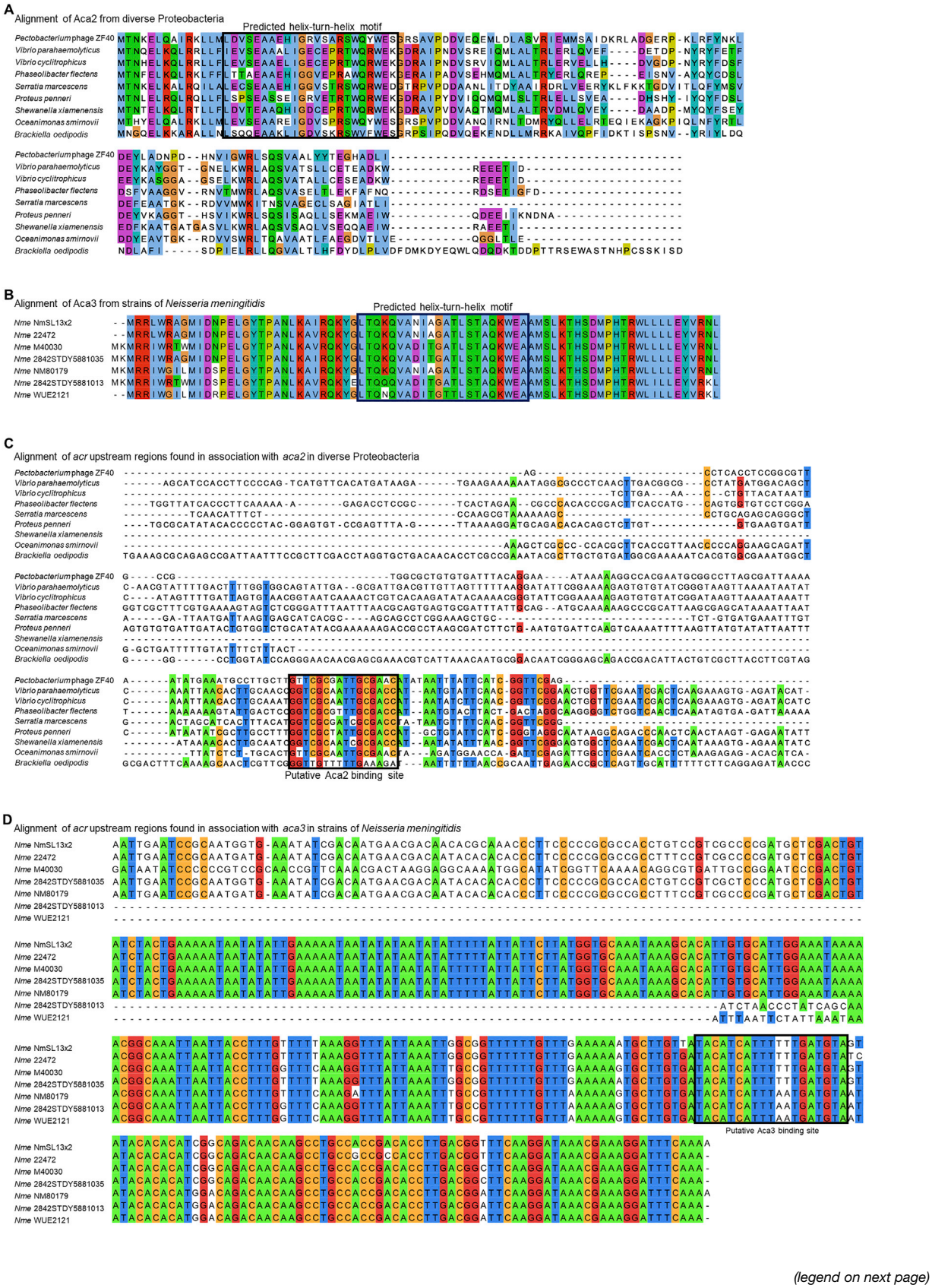

(legend on next page)

Figure S6. Multiple Sequence Alignment of Other Aca Proteins and Their Respective Anti-CRISPR Upstream Regions, Related to Figure 6

(A) Multiple sequence alignment of Aca2 proteins from diverse Proteobacteria. The predicted helix-turn-helix motif is outlined in a black box. (B) Multiple sequence alignment of Aca3 proteins from different strains of *Neisseria meningitidis*. The predicted helix-turn-helix motif is outlined in a black box. (C) Multiple nucleotide sequence alignment of the region immediately upstream of the anti-CRISPR genes found in association with *aca2* in panel A. A putative Aca2 binding site is outlined in a black box. Positions with $\geq$ 60% identity are colored (D) Multiple nucleotide sequence alignment of the region immediately upstream of the anti-CRISPR genes found in association with *aca3* in panel B. A putative binding site for Aca3 is outlined in a black box. Nme, *Neisseria meningitidis;* numbers indicate strain. Positions with > 60% identity are colored. See also Table S3.

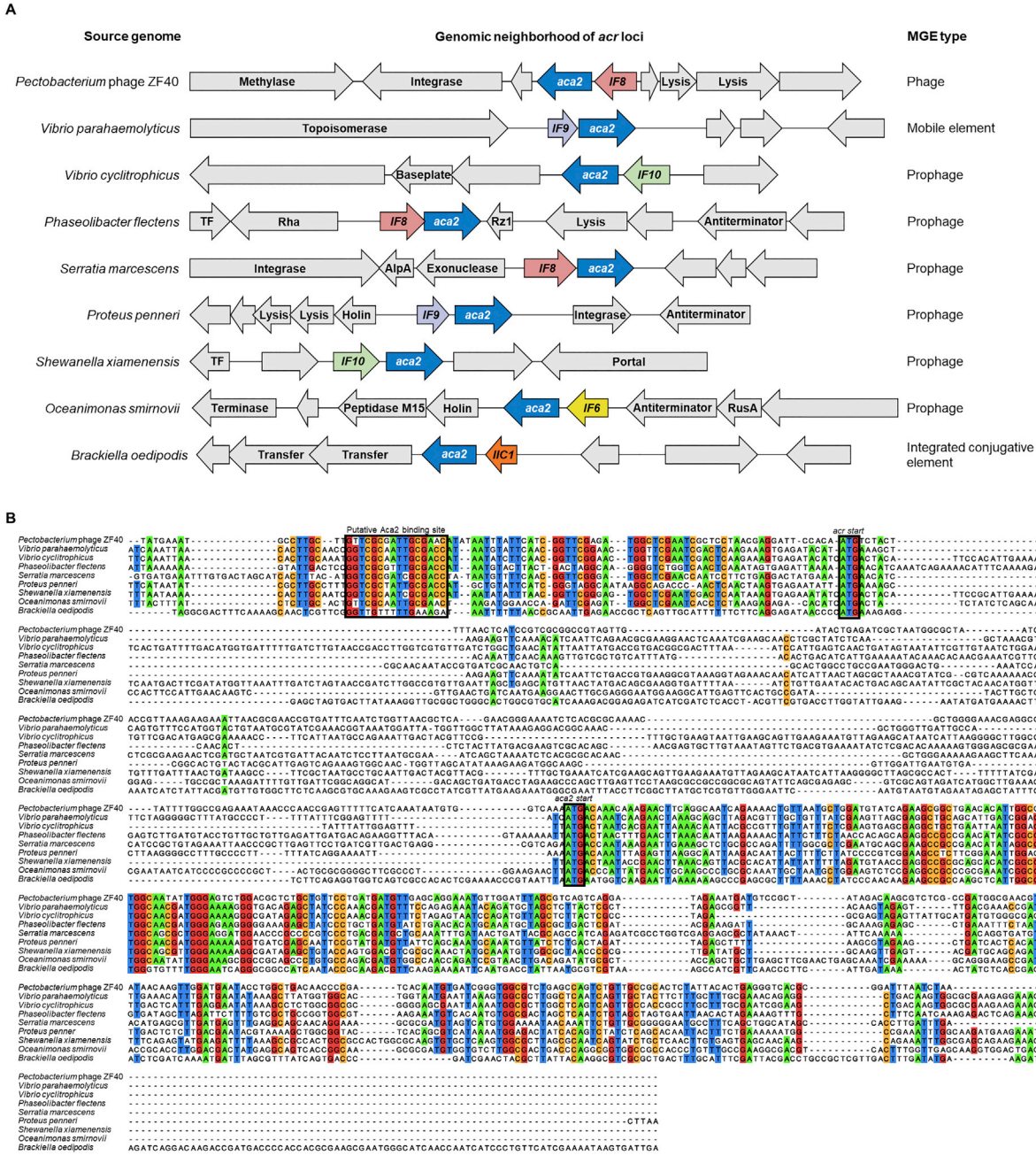

Figure S7. *aca2* Genes Found in Diverse Genomic Contexts Share Conserved Sequences, Related to Figures 1 and S6

(A) Schematic representation of the genomic context of *aca2*-associated anti-CRISPR operons. Colored arrows represent anti-CRISPR and anti-CRISPR-associated (*aca*) genes. Genes shown in gray represent the genomic context. Predicted functions are indicated when known. Arrows representing genes are not shown to scale. TF = transcription factor. Anti-CRISPR genes are denoted as *IX#*, where I represents the type of system targeted, X represents the subtype of system targeted, and # represents the protein family. (B) Multiple nucleotide sequence alignment of the region immediately upstream of the anti-CRISPR genes found in association with *aca2* to the stop codon of *aca2*. A putative *aca2* binding site as well as the *acr* and *aca2* start codon are outlined in black boxes. Positions sharing ≥ 60% identity are colored. See also Table S3.